UBXN1 maintains ER proteostasis and represses UPR activation by modulating translation independently of the p97 ATPase

Brittany A. Ahlstedt[1], Rakesh Ganji[1], Sirisha Mukkavalli[1*], Joao A. Paulo[2], Steve P. Gygi[2], and Malavika Raman[1#]

[1] Department of Developmental Molecular and Chemical Biology, Tufts University School of Medicine, Boston MA.

[2] Department of Cell Biology Harvard Medical School, Boston MA.

* Present address Dana Farber Cancer Research Institute, Boston MA.

Address correspondence to Malavika Raman, malavika.raman@tufts.edu

Abstract

Endoplasmic reticulum (ER) protein homeostasis (proteostasis) is essential to facilitate proper folding and maturation of proteins in the secretory pathway. Loss of ER proteostasis due to cell stress or mutations in ER proteins can lead to the accumulation of misfolded or aberrant proteins in the ER and triggers the unfolded protein response (UPR). In this study we find that the p97 adaptor UBXN1 is an important negative regulator of the UPR. Loss of UBXN1 significantly sensitizes cells to ER stress and activates canonical UPR signaling pathways. This in turn leads to widespread upregulation of the ER stress transcriptional program. Using comparative, quantitative proteomics we show that deletion of UBXN1 results in a significant enrichment of proteins belonging to ER-quality control processes including those involved in protein folding and import. Notably, we find that loss of UBXN1 does not perturb p97-dependent ER associated degradation (ERAD). Our studies indicate that loss of UBXN1 increases translation in both resting and ER-stressed cells. Surprisingly, this process is independent of p97 function. Taken together, our studies have identified a new role for UBXN1 in repressing translation and maintaining ER proteostasis in a p97 independent manner.

53 **Introduction**

54 The ER is a major site for protein maturation and oversees the folding and secretion of
55 one-third of the cellular proteome. A tight equilibrium exists between the ER protein folding
56 capacity and protein load to maintain ER proteostasis. Alterations in this equilibrium due to various
57 physiological conditions such as disruption of ER-calcium homeostasis, mutations that impair
58 protein folding, or cellular aging can result in protein misfolding[1]. ER stress is elicited by protein
59 misfolding and aggregation and can become pathological if not alleviated. Indeed, protein
60 misfolding and aggregation are hallmarks of many age-associated neurodegenerative disorders.
61 Numerous studies indicate that in neurodegenerative disorders such as Parkinson's Disease (PD)
62 and amyotrophic lateral sclerosis (ALS), age associated protein aggregation in the ER is causally
63 linked to cell death[2-5]. Protein aggregates can inappropriately interact with ER chaperones,
64 disrupting ER morphology and vesicular trafficking to the Golgi apparatus[6-8]. In the context of
65 these age-related disorders, it is known that a decline in the efficiency and capacity of protein
66 quality control systems diminishes ER-protein homeostasis. However, it is currently unclear how
67 decline in specific protein quality control mechanisms impacts cell health. Recent studies suggest
68 that aging cells rewire chaperone subnetworks and find that proteasome and autophagy
69 capacities are altered[9-11]. Thus, a thorough understanding of protein quality control mechanisms
70 is warranted to comprehend how their decline triggers disease onset.

71 Distinct ER-quality control mechanisms sense ER stress. These include the unfolded
72 protein response (UPR) and ER-associated degradation (ERAD) which function to improve the
73 folding capacity of the ER, and clear misfolded proteins from the ER through the ubiquitin-
74 proteasome system respectively. The UPR is an adaptive ER-quality control pathway comprised
75 of three, parallel, ER-resident transmembrane stress sensors that monitor the misfolded protein
76 burden within the ER**.** These sensors include activating transcription factor 6 (ATF6), inositol
77 requiring enzyme 1 (IRE1), and protein kinase R (PKR)-like ER kinase (PERK). Signaling
78 pathways downstream of each sensor ultimately activates a distinct transcription factor that

79 induces the expression of a suite of UPR-specific target genes, encoding chaperones and protein
80 degradation machinery[12]. The prevailing theory suggests that the ER sensors are held in an
81 inactive state when their luminal domains are bound to the abundant ER chaperone, binding
82 immunoglobulin protein (BiP) (also known as glucose-regulated protein 78 kDa, GRP78)[13]. When
83 misfolded proteins accumulate, BiP is titrated away from the sensors, triggering their
84 activation[14,15]. Under these conditions, ATF6 traffics from the ER to the Golgi apparatus where
85 site-1 and site-2 proteases release the cytosolic domain of ATF6 to generate an active
86 transcription factor. In contrast, PERK dimerizes upon activation and phosphorylates eukaryotic
87 initiation factor 2α (eIF2α), diminishing the translation initiation of most proteins[16]. In response to
88 eIF2α phosphorylation, the translation of activating transcription factor 4 (ATF4) is selectively
89 induced in response to reinitiation of ribosomes at the upstream *atf4* coding region. Lastly, IRE1
90 forms oligomers and mediates the unconventional mRNA splicing of an intron from the x-box
91 binding protein-1 (*xbp1*) mRNA to generate the active transcription factor xbp1s[17,18]. Additionally,
92 IRE1 degrades ER-targeted mRNAs in a process termed regulated IRE1-dependent decay
93 (RIDD)[19]. The rapid degradation of mRNAs through RIDD functions to alleviate ER stress by
94 preventing the continued influx of new polypeptides into the ER[20,21]. If these mechanisms fail to
95 alleviate ER stress, PERK and IRE1 signaling will induce apoptosis through expression of the
96 pro-apoptotic transcription factor C/EBP homologous protein (CHOP) and JNK signaling
97 respectively[22-24].

98 The UPR works in tandem with ERAD which purges terminally misfolded clients from the
99 ER by the ubiquitin-proteasome system. During ERAD, misfolded ER proteins are recognized and
100 handed off to ER membrane resident E3 ligases to initiate ubiquitin-dependent degradation by
101 cytosolic proteasomes. The AAA+ ATPase p97 (also known as valosin containing protein, VCP)
102 is a critical intermediate in this process that recognizes ubiquitylated proteins and retro-
103 translocates them from the ER to the cytosol prior to proteasomal degradation. The p97 homo-
104 hexamer utilizes ATP hydrolysis to unfold substrates[25-27] and participates in an array of cellular

105 pathways from the cell cycle to autophagy[28,29]. p97 interacts with a variety of dedicated adaptor
106 proteins that facilitate substrate specificity and targeting of p97. The largest family of p97 adaptors
107 contain a ubiquitin regulatory X (UBX) domain that enables binding to p97[30]. Many of the UBX
108 domain containing adaptors also harbor a ubiquitin associated domain (UBA) that associates with
109 polyubiquitin chains on client proteins. There are ~40 adaptors, though the functions and
110 substrates of most remain poorly characterized. Studies have shown that p97 mutation can
111 disrupt p97-adaptor binding which has been causally linked to multisystem proteinopathy 1 (MSP-
112 1), a degenerative disorder wherein individuals present with inclusion body myopathy, Paget's
113 disease of the bone and/or frontotemporal dementia[31-35]. More recently, p97 mutation has been
114 linked to the development of familial ALS (fALS), PD, and Charcot-Marie-Tooth disease type IIB
115 (CMTIIB)[36-39]. A full understanding of adaptor function is required to better understand how their
116 dysfunction disrupts protein quality control pathways to contribute to disease pathogenesis.

117 In a previous study, we reported that the p97 adaptor UBX domain protein 1 (UBXN1)
118 associated with the multifunctional BCL2-associated athanogene 6 (BAG6) chaperone. BAG6
119 facilitates the insertion of tail anchored proteins into the ER[40-45]. When clients fail to insert (due to
120 mutations, saturation of insertion machinery at the ER, or ER stress), BAG6 recruits the E3 ligase
121 RNF126 for ubiquitylation and degradation of the substrate[44]. We showed that UBXN1 was
122 important for the recruitment of p97 to the BAG6 triage complex to facilitate extraction and
123 degradation of non-inserted substrates. In addition, BAG6 has also been reported to function in
124 ERAD in concert with p97 by acting as a chaperone 'holdase' for unfolded p97 clients[46-48].
125 However, our studies indicated that UBXN1 is not a ERAD adaptor for p97[40]. Here, we have
126 identified a novel role for UBXN1, as a regulator or ER proteostasis. In this study, we demonstrate
127 that cells depleted of UBXN1 have elevated UPR activation both in unperturbed and ER-stressed
128 cells. Using quantitative proteomics, we find a significant increase in the abundance of ER
129 proteins in UBXN1 deleted cells. Increased steady state protein levels are not due to the
130 participation of UBXN1 in p97-dependent ERAD. We further demonstrate that loss of UBXN1

131 increases protein translation in a p97-independent manner and this may be the cause of ER
132 stress. Our studies have identified a new regulator of protein translation and ER proteostasis.
133
134 **Results**
135 **UBXN1 depletion induces activation of the unfolded protein response.**
136 Based on our prior study on p97-UBXN1 regulation of BAG6-associated protein triage, we
137 presumed that one consequence of UBXN1 loss may be imbalance in the ER proteome and
138 subsequent ER stress. Indeed, loss of p97 or BAG6 function can cause the accumulation of
139 misfolded proteins in the ER via multiple mechanisms to activate the UPR. Silencing BAG6 with
140 siRNA or inhibiting p97 with the ATP-competitive inhibitor CB-5083 caused robust activation of
141 the UPR as expected by immunoblotting for the ER chaperone BiP and transcription factor ATF4
142 (Supplementary Figure 1 A-E). To assess if UBXN1 was also involved in ER stress responses,
143 we systematically assessed UPR activation in UBXN1 knock-out (KO) HeLa Flp-In T-REx (HFT)
144 cell lines generated by CRISPR-Cas9 gene editing. Wildtype and UBXN1 KO cells were treated
145 with the reducing agent dithiothreitol (DTT), and lysates were probed for the ER chaperone BiP,
146 the transcription factor ATF4, and phosphorylation of eIF2α (Figure 1A and B). In wildtype cells,
147 a time-dependent increase in these proteins was observed, however a significant increase was
148 apparent at earlier time points in UBXN1 KO cells. Notably, these markers were already
149 upregulated in untreated UBXN1 KO cells (Figure 1A, compare lane 5 and 1). We next monitored
150 the levels of cleaved ATF6 in wildtype and UBXN1 KO cells treated with DTT. Cells were co-
151 treated with the proteasome inhibitor Bortezomib (BTZ) to prevent turnover of and facilitate
152 visualization of the N-terminus of ATF6[49]. Compared to control cells, there was a modest but
153 significant increase in cleaved ATF6 in UBXN1 KO cells in response to ER stress (Figure 1C and
154 D). Under ER stress conditions, IRE1α is activated by dynamic clustering in the ER
155 membrane[50,51]. IRE1α monomers cluster into higher order oligomers that can be imaged and

156 quantified by immunofluorescence. We generated a stable cell line using a previously published
157 doxycycline-inducible GFP-tagged IRE1α reporter to observe IRE1α clustering[51]. Utilizing this cell
158 line, IRE1 clustering into oligomers was quantified by quantifying the number of GFP puncta.
159 UBXN1 was depleted with two independent siRNAs and cells were imaged for GFP-foci (Figure
160 1E). We found that 40% of cells depleted of UBXN1 contained GFP-IRE1α foci compared to the
161 10% observed in cells transfected with a control siRNA (Figure 1F). Furthermore, there were
162 significantly more GFP-foci per cell in UBXN1-depleted cells compared to control (Figure 1F).
163 Additionally, we measured IRE1 activation via downstream *xbp1s* expression in UBXN1 KO cells
164 by quantitative real-time PCR using a primer set that spans the splice site removed by IRE1α[52].
165 We detected 19-fold greater *xbp1s* expression in UBXN1 KO cells compared to control in
166 response to stress, while total *xbp1* levels remained unchanged (Figure 1G). A similar phenotype
167 was observed in UBXN1 KO HEK-293T cells, (Supplementary Figure 1F). Notably, the repression
168 of ER stress by UBXN1 is not due to a role for UBXN1 as a p97 adaptor for ERAD[40,53]. Using a
169 panel of GFP-tagged ERAD reporters we have previously shown that p97 and its adaptor UBXD8
170 but not UBXN1 is required for the turnover of multiple ERAD substrates[40].

171 Our group recently reported that the p97-UBXN1 complex was required for recognizing
172 ubiquitylated protein aggregates and consolidating them in a perinuclear structure known as the
173 aggresome[54]. ERAD substrates can also be recruited to these aggregates that can associate with
174 the ER membrane to cause ER stress. To determine whether UPR activation caused by UBXN1
175 loss was due to the accumulation of ubiquitylated aggregates we treated wildtype and UBXN1 KO
176 cells with ER stressors tunicamycin (Tu), which inhibits the first step in N-linked glycosylation, or
177 thapsigargin (Tg), which inhibits the endoplasmic reticulum Ca^{2+} ATPase. Cells were also treated
178 with Bortezomib to induce aggresomes as a positive control. We visualized ubiquitylated proteins
179 by microscopy and immunoblotting. Bortezomib-treated cells contained a single ubiquitin-positive
180 aggresome that was disrupted in UBXN1 KO cells as we previously reported[54]. However, wildtype

181 and UBXN1 KO cells treated with Tu or Tg had no ubiquitin positive aggregates or overt
182 accumulation of ubiquitylated proteins (Supplementary Figure 1G and H). Thus, UPR activation
183 upon UBXN1 deletion is not due to mishandling of aggregates destined for the aggresome. Taken
184 together, our findings implicate UBXN1 as a novel regulator of the UPR independent of ERAD.
185

186 **Loss of UBXN1 activates an ER stress-related transcriptional program leading to cell**
187 **death.**

188 The UPR ultimately terminates in a transcriptional response downstream of ATF4, ATF6-
189 N, and xbp1s, therefore, we analyzed UPR target gene expression using quantitative real-time
190 PCR of 84 UPR-specific target genes (Supplementary Table 1). Gene expression analysis in
191 wildtype and UBXN1 KO cells identified a global upregulation (88%, 74 of 84 targets) of UPR-
192 specific target genes in UBXN1 KO cells with 40 genes (47%) experiencing a $\log_2$ fold change $\geq$
193 0.5 (Figure 2). While this appears to be a modest change, previous microarray analysis has
194 demonstrated that only a handful (22 out of 1868 analyzed) of UPR related genes have 2-fold
195 induction in HeLa cells stressed with tunicamycin[55]. Of the genes that demonstrated a $\log_2$ fold
196 change $\geq$ 0.5, there are known targets of each of the UPR sensors, including PERK (*ddit3/chop*),
197 ATF6 (calreticulin, *(calr*) and *herpud1*), and IRE1 (*sec62* and *edem3*), among others[12,56].
198 Hierarchical clustering analysis demonstrates that the gene expression pattern observed in
199 UBXN1 KO cells more closely resembles wildtype cells stressed with DTT than untreated wildtype
200 cells based on similar $\log_2$ fold change values (Figure 2). Additionally, we observed that the
201 transcriptional response in UBXN1 KO cells treated with DTT is comparable to wildtype cells
202 treated with DTT (Figure 2). We attribute this to a ceiling effect that is often seen with UPR target
203 gene expression upon ER stress[57,58].

204 UPR signaling during acute ER stress is a protective mechanism, whereas chronic ER
205 stress and UPR activation primes cells toward apoptosis[59-62]. We assessed recovery from ER

206 stress in wildtype and UBXN1 KO cells. Cells were treated with thapsigargin for a time-course
207 spanning 0.5 to 3 hours and released into drug-free media (Figure 3A). Viable cells remaining
208 after three days were stained with crystal violet and quantified. We observed significantly reduced
209 growth of UBXN1 KO cells relative to wildtype cells suggesting that elevated UPR signaling
210 primes UBXN1 KO cells for apoptosis (Figure 3A and B). In agreement with this finding, we
211 observed that UBXN1 KO cells have elevated levels of the apoptosis inducing transcription factor
212 C/EBP homologous protein (CHOP) compared to wildtype cells in response to DTT (Figure 3C
213 and D). Thus, UBXN1 loss is detrimental to cell viability in the face of ER stress.
214

215 **Loss of UBXN1 leads to a perturbed ER proteome**

216 To understand how UBXN1 loss causes ER stress, we first asked if UBXN1 was
217 associated with the ER. We isolated ER-derived microsomes by biochemical fractionation from
218 HEK293T cells and subjected the microsomes to proteinase K digestion in the presence and
219 absence of detergent (Triton X-100) (Figure 3E). As previously reported, a significant fraction of
220 p97 is peripherally associated with the ER to regulate ERAD[63,64] and this localization is sensitive
221 to Proteinase K (Figure 3E). Similarly, we found that UBXN1 was also associated with the ER
222 membrane and was readily digested in Proteinase K treated samples (Figure 3E). We next asked
223 if UBXN1 associated with the SEC61 translocon to regulate import of proteins into the ER,
224 however in co-immunoprecipitation studies we were unable to discern an interaction between
225 UBXN1 and the translocon components SEC61α or β, whereas UBXN1 interacted with p97 as
226 expected (Supplementary Figure 2A and B).

227 We decided to take an unbiased approach to assess how UBXN1 deletion impacted ER
228 protein homeostasis. We employed quantitative tandem mass tag (TMT) proteomics. Peptides
229 derived from duplicate wildtype and UBXN1 KO cells were labelled with four-plex TMT labels,
230 combined and peptide abundance was quantified by liquid chromatography and mass
231 spectrometry (Figure 4A). We quantified a total of 6,673 proteins from this study of which 53 were

232 significantly enriched in UBXN1 KO cells (log_2 fold change KO:WT ≥ 1.0 and p ≤ 0.5) (Figure 4B,
233 Supplementary Table 2). Strikingly, gene ontology analysis identified significant enrichment of ER
234 proteins involved in protein folding, ER-quality control, and the response to ER stress (Figure 4B,
235 C, Supplementary Figure 3A, B). These include proteins involved in *N*-linked glycosylation
236 (glycosyltransferase enzymes ALG1, 3, and 5), ERAD (HRD1 E3 ligase adaptor SEL1L and the
237 ER-anchored protein escortase TMUB1[65]), and ER import (components of the heterotrimeric
238 SEC61 complex: SEC61A1, SEC62, and SEC63 and the ER membrane complex, EMC) (Figure
239 4C and Supplementary Figure 3A). Notably, when we categorized proteins based on their
240 organelle enrichment, we found that ER proteins in particular were increased in abundance
241 relative to all other organelles (Figure 4D). In contrast, mitochondrial proteins were depleted in
242 UBXN1 KO cells (Figure 4D). Thus, UBXN1 localizes to the ER and loss of UBXN1 alters protein
243 abundance within the ER.
244
245 **Depletion of UBXN1 increases the expression and aggregation of ER-destined proteins**
246 **without preventing their degradation.**
247 To further validate our proteomic studies, we examined the expression of significantly
248 enriched proteins by immunoblotting lysates from wildtype and UBXN1 depleted cells. In
249 agreement with the proteomic data, we observed a significant increase in the abundance of the
250 translocon associated protein α (TRAPα) and alkaline phosphatase placenta-like 2 (ALPP2)
251 (Figure 5A, B, and G). Interestingly, we found that this phenotype extends beyond our proteomics
252 hits; we detected a significant increase in the abundance of ER-targeted proteins α-galactosidase
253 (AGAL)[66] and Prion protein (PrP)[44] in cells transfected with the corresponding epitope tagged
254 constructs and depleted of UBXN1 (Figure 5C, 5G, Supplementary Figure 4A-C). The elevated
255 levels of these proteins are not due to increased transcription as *prp* transcript levels were
256 unchanged between wildtype and UBXN1 KO cells (Supplementary Figure 4C). We asked if the

257 elevated levels of AGAL and PrP represented ER imported forms or was due to inefficient
258 cytosolic degradation in the absence of UBXN1. We first monitored the glycosylation status of
259 FLAG-AGAL and HA-PrP. AGAL glycosylation was verified by EndoH treatment of cell lysates
260 that resulted in a faster migrating band (Supplementary Figure 4D). HA-PrP glycosylation could
261 be discerned by three distinctly migrating bands representing the unmodified, ER-resident, and
262 fully glycosylated post-ER forms (Supplementary Figure 4A). While UBXN1 depletion resulted in
263 increased steady state levels of these proteins, it did not impact the glycosylation of these proteins
264 indicating that they were targeted appropriately to the ER (Figure 5C, Supplementary Figure 4A,
265 B).

266 Next, we monitored the degradation of HA-PrP and FLAG-AGAL in wildtype and UBXN1
267 depleted cells. HA-PrP has a weak signal sequence and is mislocalized and degraded prior to
268 import in response to ER stress[44,46,67]. This can be visualized by the accumulation of a non-
269 glycosylated cytosolic from in immunoblots (Supplementary Fig 4A). Cells expressing HA-PrP
270 were treated with thapsigargin and the proteasome inhibitor Bortezomib to induce mislocalization
271 and prevent degradation respectively[67]. UBXN1 depletion did not induce greater mislocalization
272 and degradation of HA-PrP relative to total protein (Supplementary Figure 4A compare lane 8 to
273 4). Furthermore, UBXN1 depletion did not prevent the turnover of FLAG-AGAL or HA-PrP
274 monitored by cycloheximide chase studies (Supplementary Figure 4E-G). UBXN1 depleted cells
275 had significantly higher levels of AGAL compared to control cells to begin with (Figure 5C, 5G,
276 Supplementary Figure 4E), but AGAL was efficiently degraded in both control and UBXN1
277 depleted cells (Supplementary Figure 4E and F). We note that at earlier timepoints, there was a
278 delay in AGAL degradation in UBXN1-depleted cells and we attribute this to the overall increase
279 in protein abundance of AGAL when UBXN1 is depleted (Figure 5C, 5G). We also assessed the
280 turnover of TRAPα and ALPP2 but these proteins had long half-lives and did not appreciably turn
281 over after 9 hours of cycloheximide treatment. Nevertheless, increased protein abundance was
282 obvious (Supplementary Figure 4H).

283 We asked if increased levels of these protein in the ER impacted their solubility. We
284 monitored AGAL solubility in control and UBXN1-depleted cells treated with DTT and fractionated
285 into soluble and insoluble fractions. In control cells, AGAL was soluble and was not found in the
286 insoluble fraction even upon DTT treatment (Supplementary Figure 4I compare lanes 1 to 3 to 7).
287 Strikingly, in cells depleted of UBXN1 and treated with DTT, AGAL shifted completely into the
288 insoluble fraction (Supplementary Figure 4I compare lanes 2 to 4 and 8).

289 We were next interested if increased protein abundance upon UBXN1 depletion was
290 unique to ER proteins as suggested by the proteomics (Figure 4D). Our proteomics study
291 identified several mitochondrial proteins depleted in UBXN1 KO cells, but no change in other
292 organellar proteins (Figure 4D). Therefore, we investigated by immunoblot if loss of UBXN1
293 impacted cytosolic, nuclear, or mitochondrial proteins. While we observed no change in the
294 abundance of proteins in the cytosol or nucleus (Supplementary Figure 4J-M), we observed a
295 significant decrease in the expression of several mitochondrial proteins when UBXN1 was
296 depleted (for example, the mitochondrial outer membrane translocon component TOMM20 and
297 the complex III subunit CYC1) (Figure 5D-G, Figure 4D). Previous studies have demonstrated
298 that the physical interaction between the ER and mitochondria at contact sites facilitates the
299 transmission of ER stress to the mitochondria[68,69]. To prevent mitochondrial dysfunction
300 transmitted by ER stress, translational attenuation through eIF2α phosphorylation mediates the
301 protective degradation of the TIMM17A subunit of the TIMM23 import complex to prevent protein
302 import into mitochondria[70]. Whether other mitochondrial proteins are similarly downregulated is
303 unknown, but our studies suggest that loss of UBXN1 differentially regulates mitochondrial protein
304 levels in response to ER stress.

305 Taken together, loss of UBXN1 increases the abundance of ER proteins and leads to their
306 aggregation upon ER stress.

307

308 **UBXN1 represses protein translation**

309 Our findings thus far suggested that loss of UBXN1 increased ER protein abundance in a
310 degradation independent manner. We therefore asked if UBXN1 directly impacted protein
311 synthesis. We utilized puromycin incorporation into newly synthesized proteins as a proxy for
312 translation[71]. Puromycin is structurally similar to aminoacyl-tRNAs and can occupy the acceptor
313 (A) site on a ribosome to be incorporated into the nascent polypeptide[72,73]. Puromycilated proteins
314 are pre-maturely released from the ribosome and can be visualized by immunoblotting with a
315 puromycin antibody[74]. Wildtype and UBXN1 KO cells were briefly labelled (~30 min) with
316 puromycin, and the levels of puromycilated proteins were quantified. We observed a significant
317 increase in puromycilated proteins in UBXN1 KO cells suggestive of increased translation (Figure
318 6A, B and Supplementary Figure 5A). We additionally treated cells with DTT or thapsigargin to
319 induce ER stress and shut down protein translation through eIF2α phosphorylation. DTT,
320 thapsigargin, or cycloheximide treatment resulted in a complete shutdown of protein synthesis in
321 wildtype cells as evidenced by the loss in puromycin signal (Figure 6A, compare lanes 7 and 5 to
322 3, Supplementary Figure 5B compare lanes 3 to 1). However, although significantly reduced in
323 UBXN1 KO cells, translation could still be observed (Figure 6A, B, Supplementary Figure 5A, B).
324 To assess the role of p97 in this process, we performed these studies in cells depleted of p97.
325 Surprisingly, we found that loss of p97 did not impact translation (Figure 6C). In fact, in p97-
326 depleted and thapsigargin treated cells, there was an even more robust termination of translation
327 compared to control cells (Figure 6C and D).

328 To determine the specificity of the phenotype, we next asked if we could rescue the
329 perturbed translation phenotype by re-expressing wildtype Myc-UBXN1 in UBXN1 KO cells. As
330 seen in Figure 6E, transfection of Myc-UBXN1 (but not Myc-GFP control) restored translation to
331 wildtype levels (Figure 6E, compare lanes 3 and 4 to lane 1). However, expressing UBXN1
332 containing mutations in the UBX domain (Phe^{265} Pro^{266} Arg^{267} truncated to Ala-Gly) that we have
333 shown previously to disrupt interaction with p97[54], also rescued the increase in protein synthesis
334 (Figure 6E and F, compare lanes 5 to 1). However, a UBXN1 UBA domain mutant (Met^{13} and

335 Phe[15] to Ala) that fails to interact with ubiquitin[40,54], did not rescue the increase in protein synthesis
336 to levels observed in wildtype levels (Figure 6E and F compare lanes 6 to 1).
337 To further confirm the increased translation phenotype, we isolated polysomes to directly
338 analyze the amount of actively translating ribosomes present on mRNA. Inhibiting protein
339 synthesis with cycloheximide halts ribosomes on mRNA such that they can be isolated by sucrose
340 gradient centrifugation and quantified. We found that UBXN1 KO cells have an increase in the
341 levels of actively translating polysomes compared to wildtype cells (Figure 6G). Strikingly, while
342 DTT treatment in wildtype cells halted protein synthesis and collapses polysomes to 80S
343 monosomes, translation persists in UBXN1 KO cells (Figure 6G). In agreement with our
344 puromycin incorporation data, depletion of p97 decreased polysomes in untreated cells that was
345 further depleted upon DTT treatment (Supplementary Figure 5C and D). Taken together UBXN1
346 represses translation in a p97-independent but ubiquitin-dependent manner (Figure 7).
347
348 **Discussion**
349 Cellular stress can provoke an imbalance between the protein folding machinery and ER-
350 protein load. Numerous studies have illuminated how protein misfolding and consequent ER
351 stress is a major disease mechanism that exacerbates the pathogenesis of a variety of disease
352 states. Failure to adapt to ER stress has been linked to inflammation and UPR-induced apoptosis
353 in cardiovascular disease, liver fibrosis, and diabetes mellitus[75-78]. Thus, it is critical to understand
354 the protein quality control mechanisms that function to prevent ER stress and maintain ER
355 proteostasis to prevent disease.
356 In the current study, we have identified a novel role for the p97 adaptor protein UBXN1 in
357 ER-quality control as a repressor of the UPR (Figure 7). We found that cells devoid of UBXN1
358 have significant activation of pathways downstream of PERK, IRE1, and ATF6 (Figure 1) resulting
359 in a transcriptional program to reset ER proteostasis (Figure 2). Our proteomic studies indicate
360 that UBXN1 KO cells have a perturbed ER-proteome with an enrichment of proteins involved in

361 protein translocation into the ER, protein folding, ER-quality control, and the response to ER
362 stress (Figure 4). The increased abundance of these ER proteins is not due to defective
363 degradation via ERAD (Supplementary Figure 4). Furthermore, increased protein abundance in
364 the ER triggers aggregation as observed with AGAL. We propose that the increased influx of
365 proteins into the ER in UBXN1 KO cells causes UPR activation.

366 A recent study reported that re-initiation of protein synthesis before the restoration of ER
367 proteostasis can induce cell death in response to ER stress[60]. This study found that forced CHOP
368 and ATF4 expression after ER stress induces the expression of several aminoacyl-tRNA
369 synthetases and ribosomal proteins leading to increased translation. Increased protein synthesis
370 elevated reactive oxygen species (ROS) to trigger ER-stress induced apoptosis[60,61]. Therefore,
371 the ability to attenuate protein synthesis is paramount to cell viability. Indeed, MEFs harboring an
372 S51A mutation in eIF2α which prevents phosphorylation of eIF2α by PERK were significantly
373 sensitized to ER stress, whereas ATF4 null cells, which more slowly restored protein synthesis,
374 were resistant to ER-stress induced cell death[60]. We find robust elevation in the levels of ATF4
375 (Figure 1) and CHOP (Figure 3) in UBXN1 null cells and these cells are more sensitive to ER
376 stress than their wildtype counterparts (Figure 3).

377 Finally, we show that UBXN1 is a translation repressor and loss of UBXN1 increases
378 protein translation under basal conditions and in response to ER stress. Whether this occurs
379 through increased ATF4 expression is under investigation. Our study does not address whether
380 ER proteins are specifically repressed by UBXN1 or if it represses translation globally. However,
381 our analysis of the proteomic results and validation studies suggest that ER proteins in particular
382 are more abundant in UBXN1 deleted cells (Figure 4 and 5). How UBXN1 represses translation
383 is currently under investigation.

384 Surprisingly, we observed that the role of UBXN1 in repressing protein translation is
385 independent of p97 function but reliant on its ability to bind ubiquitin (Figure 6). p97 adaptors are
386 often thought to function exclusively in complex with p97, however, some studies suggest that

387 UBXN1 may function in the absence of p97. For example, after infection by RNA viruses, RIG-I-
388 like receptors in the cytoplasm bind to mitochondrial-antiviral signaling protein (MAVS) to rapidly
389 induce the expression of type I interferons (IFNs)[79]. UBXN1 is recruited to MAVS where it sterically
390 inhibits the binding of downstream effector molecules that contribute to IFNs production[80]. This
391 function was found to be p97 independent as p97 depletion with siRNA, or mutation of the UBX
392 domain did not impact suppression of these pathways. Only the UBA domain was shown to be
393 necessary and sufficient to inhibit antiviral signaling[80,81]. Whether other adaptors have functions
394 independent of the p97 ATPase remains to be elucidated.

395 Emerging studies indicate the presence of "pre-emptive" ER-quality control systems that
396 preclude protein misfolding in the ER by preventing the insertion of aberrant proteins. These
397 pathways act upstream of UPR and ERAD. The BAG6-RNF126 mediated degradation of
398 mislocalized ER proteins is one such pre-emptive quality control mechanism[40,44,46,67]. Recently,
399 Ufmylation of the ribosomal protein uL24 (Rpl26) has been reported to enable the degradation of
400 stalled polypeptides in the translocon[82,83]. It is likely that multiple measures exist to maintain an
401 optimal ER proteome prior to UPR and ERAD activation but they remain to be fully elucidated.
402 We propose that UBXN1-mediated translation repression is one such measure that warrants
403 further investigation.

404

405 **FIGURE LEGENDS**

406 **Figure 1. UBXN1 depletion induces activation of the unfolded protein response.**
407 **(A)** Immunoblot of HFT wildtype and UBXN1 KO cells treated with 1.5 mM dithiothreitol (DTT) for
408 the indicated timepoints (0-8 hours) to visualize downstream PERK targets. **(B)** Ratio (UBXN1
409 KO/wildtype) of the band intensity quantifications of BiP, ATF4, and peIF2α at the 8-hour timepoint
410 corresponding to Figure 1A. (*n* = three biologically independent samples). We only provide the 8-
411 hour quantification as the signal is not present in wildtype cells in earlier timepoints for accurate
412 quantification. **(C)** Immunoblot of HFT wildtype and UBXN1 KO cells co-treated with 1.5 mM DTT

413 and 1 μM Bortezomib (BTZ) to visualize full-length and cleaved ATF6. **(D)** ATF6 activation was
414 measured by band intensity quantification and calculation of the percentage of cleaved ATF6 to
415 total ATF6. The ratio of the percentage of ATF6 activation in UBXN1 KO cells to wildtype is
416 reported. (*n* = four biologically independent samples). **(E)** Representative immunofluorescent
417 image of IRE1α clustering in a stable, doxycycline inducible HFT cell line expressing GFP-tagged
418 IRE1α. UBXN1 was depleted by siRNA transfection and cells were treated with 2.5 μM
419 tunicamycin (Tu) for 4 hours to induce IRE1α clustering (Scale bar: 10 μm). **(F)** Quantification
420 corresponding to Figure 1E reporting the percent of cells with GFP-IRE1α foci as well as the
421 number of GFP-IRE1α foci per cell (*n* = three biologically independent samples). **(G)** Transcript
422 levels of *xbp1s* and total *xbp1* in HFT wildtype and UBXN1 KO cells quantified by real-time PCR.
423 Cells were treated with 10 nM thapsigargin (Tg) for 4 hours as indicated. (*n* = three biologically
424 independent samples). Data are means ± SEM (*, **, ***, **** where $P < 0.05$, 0.01, 0.001, and
425 0.0001, respectively.) Unpaired two-tailed *t* test **(B, D)** or One-way ANOVA with Tukey's multiple
426 comparisons test **(F, G)**.
427
428 **Figure 2. Loss of UBXN1 activates an ER stress transcriptional program.**
429 Heat map displays the hierarchical clustering of the $\log_2$ fold change of 84 UPR target genes
430 determined by the Human Unfolded Protein Response real-time PCR profiler array. The range is
431 from a $\log_2$ fold change of -2 (blue) to a $\log_2$ fold change of 4 (red). The untreated wildtype column
432 is displayed as an average of two replicates with the $\log_2$ fold change set to zero for this column.
433 Additional columns represent two replicates of untreated UBXN1 KO cells, two replicates of
434 UBXN1 KO cells treated with 1.5 mM DTT, and two replicates of HFT wildtype cells treated with
435 1.5 mM DTT for 4 hours respectively. Section 1 and 2 represent UPR target genes that experience
436 increased expression in the untreated UBXN1 KO cells as well as UBXN1 KO and wildtype cells
437 treated with DTT. Section 3 represents a set of UPR target genes that experience decreased

438 expression in all samples compared to untreated wildtype samples. Genes are color coded by the
439 upstream UPR stress sensor that induces their expression: PERK (green); IRE1 (red); ATF6
440 (blue); PERK and IRE1 (purple); ATF6 and IRE1 (orange). (*n* = two biologically independent
441 samples).
442
443 **Figure 3. UBXN1 localizes to the ER and preserves cell viability.**
444 **(A)** Cell viability of wildtype or UBXN1 KO cells was determined by crystal violet staining. Cells
445 were treated with 200 nM thapsigargin (Tg) for the indicated timepoints and released into drug
446 free media. Colonies were allowed to grow out for three days and live cells were stained with
447 crystal violet. **(B)** Percent viability calculated from the remining cells in Figure 3A. (*n* = four
448 biologically independent samples) **(C)** Immunoblot of HFT wildtype and UBXN1 KO cells treated
449 with 1.5 mM dithiothreitol (DTT) for the indicated timepoints (0-8 hours) to visualize CHOP
450 expression. **(D)** Band intensity quantifications of CHOP expression at the 8-hour timepoint
451 corresponding to Figure 3C. (*n* = three biologically independent samples)**.** We only provide the 8-
452 hour quantification as the signal is not present in wildtype cells in earlier timepoints for accurate
453 quantification. **(E)** Subcellular fractions enriched in ER-derived microsomes were isolated from
454 HEK-293T cells by biochemical fractionation. Protease protection assay was used to localize
455 UBXN1 to the ER periphery by immunoblot. Calnexin and Sec61β are ER specific markers, β-
456 actin is a cytosolic marker, and TOMM20 is a mitochondrial marker. (PNS: post-nuclear
457 supernatant sample, cyto: cytosolic sample). Data are means ± SEM (*, **, **** where $P < 0.05$,
458 0.01, and 0.0001, respectively.) Unpaired two-tailed *t* test **(B and D)**
459
460 **Figure 4. Loss of UBXN1 leads to a perturbed ER proteome.**
461 **(A)** Schematic workflow of quantitative tandem mass tag (TMT) proteomics in HFT wildtype and
462 CRISPR-Cas9 UBXN1 knock-out (KO) cells. **(B)** Volcano plot of the ($-\log_{10}$-transformed *P* value
463 versus the $\log_2$-transformed ratio of wildtype/UBXN1 KO) proteins identified by TMT proteomics

464 in wildtype and UBXN1 KO cells. A negative $\log_2$ fold change indicates proteins with increased
465 abundance in UBXN1 KO cells. Proteins with a $\log_2$ fold change $\geq |1|$ are considered significant.
466 ER membrane and luminal proteins are outlined by a red and blue circle respectively. Proteins
467 involved in translocation into the ER and glycosylation are colored in green and blue respectively
468 (*n* = 2 biologically independent samples for each genotype). **(C)** Metascape gene ontology
469 network of the proteins identified to be enriched in UBXN1 KO cells grouped by functional ontology
470 category. The size of the node represents the number of genes in that gene ontology cluster and
471 the thickness of the circle outline corresponds to the $-\log_{10}$-transformed *P* value of each term.
472 The different circle colors correspond to a specific gene ontology category. **(D)** Proteins identified
473 in the quantitative proteomics study categorized by organellar compartment. Proteins associated
474 with the ER experience a significant increase in abundance in UBXN1 KO cells where
475 mitochondrial proteins are significantly decreased. Data are means ± SEM (**** where $P <$
476 0.0001). One-way ANOVA with Brown-Forsythe and Welch ANOVA tests of -logFC **(D)**.
477
478 **Figure 5. Depletion of UBXN1 increases the expression of ER-destined proteins.**
479 **(A and B)** Representative immunoblots of proteins identified to be enriched in the proteomics
480 study. The ER and secretory proteins TRAPα and ALPP2 were measured in control cells or cells
481 depleted of UBXN1 for 48 hours with siRNA. Cells were either untreated or treated with 10 mM
482 DTT for 4 hours. **(C)** Immunoblot of a stable HFT cell line expressing doxycycline inducible FLAG-
483 tagged α-galactosidase (AGAL). UBXN1 was depleted with siRNA for 24 hours before AGAL
484 induction by 2 μg/ml doxycycline for 24 hours. Cells were untreated or treated with 10 mM DTT
485 for 4 hours. **(D-F)** Representative immunoblots of the mitochondrial resident proteins Aconitase-
486 2 (ACO2), TOMM20, and CYC1 measured in control or UBXN1 depleted cells (48 hours) either
487 untreated or treated with 10 mM DTT for 4 hours. **(G)** Band intensity quantifications of protein
488 expression corresponding to Figure 5A-F. (*n* = three biologically independent samples). Data are

489 means ± SEM (*, **, ***, **** where $P < 0.05$, 0.01, 0.001, and 0.0001, respectively.) One-way
490 ANOVA with Tukey's multiple comparisons test **(G)**.
491
492 **Figure 6. UBXN1 represses protein translation.**
493 **(A)** Representative immunoblot of puromycin incorporation into HFT wildtype and UBXN1 KO
494 cells. Cells were pulsed with 1 μM puromycin or 1 μM puromycin in combination with 10 μg/mL
495 cycloheximide (CHX) for 30 minutes. When applicable, cells were pretreated with 1.5 mM DTT
496 for 1 hour before 1 μM puromycin pulse for 30 minutes. The level of puromycin incorporation
497 reflects the rate of protein synthesis. **(B)** Puromycin, DTT, and CHX plots correspond to the
498 intensity of each lane in the immunoblot in Figure 6A. The intensity of the traces for each wildtype
499 and UBXN1 KO sample was determined by the plot profile feature in Fiji. The x-axis represents
500 the distance along the lane. **(C)** Representative immunoblot of 1 μM puromycin incorporation into
501 control cells or cells depleted of p97 with siRNA for 48 hours. Cells were either untreated or pre-
502 treated with 1 μM thapsigargin for 30 minutes. **(D)** Quantification of the whole lane corresponding
503 to each lane in the immunoblot in Figure 6C (*n* = four biologically independent samples). **(E)** Myc-
504 tagged GFP, wildtype, UBX domain mutant, or UBA domain mutant UBXN1 was expressed in
505 cells for 48 hours before 1 μM puromycin pulse for 30 minutes. **(F)** Quantification of each lane
506 intensity from Figure 6E. (*n* = three biologically independent samples) **(G)** Polysome profile traces
507 of HEK-293T wildtype and UBXN1 KO cells either untreated or treated with 2 mM DTT for 60
508 minutes. The 40S, 60S, and 80S ribosomal subunits are labeled as well as actively translating
509 polysomes. Traces below correspond to the polysomes seen in the main trace. Data are means
510 ± SEM (**** where $P < 0.0001$.) One-way ANOVA with Tukey's multiple comparisons test **(D, F).**
511
512 **Figure 7. UBXN1 represses protein translation to prevent ER stress and UPR activation.**

513 UBXN1 plays an important role in ER-quality control to maintain ER proteostasis. Loss of UBXN1
514 increases protein synthesis. Increased abundance of ER proteins leads to protein misfolding and
515 activation of the UPR.
516
517 **Supplementary Figure 1. BAG6 depletion and pharmacological inhibition of p97 induces**
518 **activation of the unfolded protein response.**
519 **(A)** Immunoblot of BiP and ATF4 expression levels in HFT wildtype cells treated with 1 μM
520 thapsigargin (Tg), 5 μM of the ATP-competitive p97 inhibitor CB-5083, or both for the indicated
521 timepoints (0-6 hours). **(B-C)** Band intensity quantifications of BiP **(B)** and ATF4 **(C)**
522 corresponding to Supplementary Figure 1A reporting the fold change compared to the untreated
523 condition (*n* = three biologically independent samples)**. (D)** Immunoblot of HFT wildtype cells
524 depleted of BAG6 with siRNA for 48 hours before treatment with 1.5 mM DTT for the indicated
525 timepoints (0-8 hours). **(E)** Band intensity quantifications of BiP and ATF4 corresponding to
526 Supplementary Figure 1D. at the 8-hour timepoint. (*n* = four biologically independent
527 experiments). **(F)** Transcript levels of *xbp1s* and total *xbp1* in HEK-293T wildtype and UBXN1 KO
528 cells quantified by real-time PCR. Cells were treated with 10 nM thapsigargin (Tg) for 4 hours as
529 indicated (*n* = three biologically independent samples). **(G)** Immunofluorescent staining of
530 ubiquitin (FK2) and nuclei (Hoechst dye) in HFT wildtype and UBXN1 KO cells. Cells were treated
531 with 1 μM of the proteasome inhibitor bortezomib (BTZ), Tunicamycin (Tu), or Thapsigargin (Tg)
532 for 8 hours or 1 μM BTZ, 500 nM Tu, or 500 nM Tg for 18 hours. **(H)** Immunoblot assessing total
533 ubiquitin levels corresponding to Supplementary Figure 1G. Data are means ± SEM (*, **, ***, ****
534 where $P < 0.05$, 0.01, 0.001, and 0.0001, respectively.) One-way ANOVA with Dunnetts's multiple
535 comparisons test **(B and C).** Unpaired two-tailed *t* test **(E).** One-way ANOVA with Tukey's multiple
536 comparisons test **(F)**.
537
538 **Supplementary Figure 2. UBXN1 does not interact with the Sec61 translocon.**

539 **(A)** Representative immunoblot for the immunoprecipitation of endogenous UBXN1 from HEK-
540 293T lysates. 10 and 20 µg of whole cell lysate was used for the input. Sec61β was used as a
541 marker for the Sec61 translocon. **(B)** UBXN1 and Sec61β were separately immunoprecipitated
542 from ER-microsomes isolated from HEK-293T cells. 10 and 20 µg of whole cell lysate was used
543 for the input.
544
545 **Supplementary Figure 3. Loss of UBXN1 leads to a perturbed ER proteome.**
546 **(A)** Interaction network of the gene ontology clusters from the wildtype/UBXN1 KO quantitative
547 proteomics study with a significant increase in abundance in UBXN1 KO cells. Proteins found in
548 each node are labelled and the color of each circle corresponds to the $-\log_{10}$-transformed *P* value.
549 **(B)** Bubble plot corresponding to significantly enriched gene ontology groups in the wildtype
550 (navy) and UBXN1 KO (teal). The size of the circle corresponds to the number of genes identified
551 in each term.
552
553 **Supplementary Figure 4. Depletion of UBXN1 increases the expression of ER-destined**
554 **proteins.**
555 **(A)** Immunoblot of HFT wildtype cells expressing HA-tagged prion protein (PrP). PrP was
556 expressed in HeLa cells for before siRNA mediated depletion of UBXN1. Cells were treated with
557 500 nM thapsigargin, 1 µM bortezomib (BTZ), or both for 16 hours. The percent mislocalization
558 was calculated from the ratio of the mislocalized (cytosolic) form to all forms of PrP for that sample.
559 **(B)** Total PrP protein expression was calculated by the sum of all forms of PrP for that sample.
560 The untreated condition was quantified (lanes 1 and 5) (*n* = three biologically independent
561 experiments). **(C)** Transcript levels of HA-PrP in cells depleted of UBXN1 quantified by real-time
562 PCR. Control is cDNA generated from cells not expressing HA-PrP. (*n* = three biologically
563 independent experiments). **(D)** Immunoblot of a stable HFT cell line expressing doxycycline

564 inducible FLAG-tagged AGAL. Glycans were digested with EndoH for 4 hours to generate the
565 non-glycosylated form. **(E)** Immunoblot examining the turnover of FLAG-AGAL in siRNA control
566 and UBXN1 depleted cells (48 hours). Cells were treated with 10 μg/mL cycloheximide (CHX) for
567 the indicated timepoints (0-9 hours). **(F)** Band intensity quantification of each time point of the
568 CHX time course corresponding to Supplementary Figure 5E. The zero hour time point was set
569 to 100 % for each siRNA and the % of AGAL remaining for each time point was quantified as a
570 ratio from the zero hour timepoint for that siRNA. ($n \geq$ three biologically independent samples. **(G)**
571 Immunoblot examining the turnover of HA-PrP in siRNA control and UBXN1 depleted cells. Cells
572 were treated with 10 μg/mL cycloheximide (CHX) for the indicated timepoints (0-8 hours). **(H)**
573 Immunoblot examining the turnover of the TMT-proteomics hits (ALPP2 and TRAPα) that were
574 identified to be significantly enriched in cells depleted of UBXN1. Control and UBXN1 depleted
575 cells were treated with 10 μg/mL cycloheximide (CHX) for the indicated timepoints (0-9 hours). **(I)**
576 Immunoblot of soluble and insoluble fractions of FLAG-tagged AGAL in control cells or cells
577 depleted of UBXN1 with siRNA. Cells were either untreated or treated with 10 mM DTT for 4
578 hours. (In this experiment only, we quantified and ran 2.5x less siUBXN1 protein so we could
579 accurately visualize and compare siControl to siUBXN1. The AGAL expression in siUBXN1 cells
580 often bleaches out what can be observed with siControl.) **(J-L)** Immunoblots of samples from
581 Figure 5A. examining the protein expression of additional organellar proteins including the nuclear
582 protein MCM3 and the cytosolic proteins G3BP1 and HPS90. **(M)** Band intensity quantifications
583 of protein expression corresponding to Supplementary Figure 5J-L. (n = three biologically
584 independent samples). Data are means ± SEM (*, **, and *** where $P < 0.05$, 0.01, and 0.001
585 respectively.) Unpaired two-tailed t test **(B and F)**, One-way ANOVA with Tukey's multiple
586 comparisons test **(C and M)**.
587
588 **Supplementary Figure 5. UBXN1 suppresses protein synthesis.**

589 **(A)** Densitometry quantifications of the entire lanes corresponding to Figure 6A ($n \geq$ three
590 biologically independent experiments). **(B)** Immunoblot of HFT wildtype and UBXN1 KO cells
591 pulsed with 1 μM puromycin for 30 minutes after pre-treatment with 1.5 μM thapsigargin for 30
592 minutes. **(C)** Polysome profile traces of HEK-293T control cells or cells depleted of p97 with siRNA
593 for 72 hours. Cells were either untreated or treated with 2 mM DTT for 60 minutes. The 40S, 60S,
594 and 80S ribosomal subunits are labeled as well as actively translating polysomes. Traces on the
595 right correspond to the polysomes seen in the traces on the left. **(D)** Immunoblot validating the
596 siRNA knockdown corresponding to Supplementary Figure 6C. Data are means ± SEM (*** and
597 **** where $P < 0.001$ and 0.0001, respectively.) One-way ANOVA with Tukey's multiple
598 comparisons test **(A)**.
599
600 **MATERIALS AND METHODS**
601 **Cell culture, transfections, immunoblot, and immunoprecipitation**
602 HeLa Flp-IN T-REX (HFT) and HEK-293T cells were cultured in Dulbecco's modified Eagle's
603 medium (DMEM) supplemented with 10 % fetal bovine serum (FBS) and 100 U/mL penicillin and
604 streptomycin. Cells were grown in a humidified, 5 % CO_2 atmosphere at 37 °C. For siRNA
605 transfections, cells were either forward or reverse transfected with 20 nM siControl, siUBXN1,
606 siBAG6, or sip97 using Lipofectamine RNAiMax (Invitrogen) in 6-well plates. After 8 or 24 hours
607 depending on the study, cells were split into 12-well plates for treatment. 48 hours post
608 transfection, cells were treated with the indicated drugs for the indicated timepoints before harvest
609 for immunoblot or fixation for immunofluorescence. For DNA transfections, 1 μg HA-prion protein
610 (PrP), 0.5 μg Myc-tagged wildtype UBXN1, 0.5 μg of either Myc-tagged UBX mutant (Phe^{265} Pro^{266}
611 Arg^{267} truncated to Ala-Gly), or Myc-tagged UBA mutant (Met^{13} and Phe^{15} to Ala), and 50 ng Myc-
612 tagged GFP constructs were forward transfected into HFT cells seeded in a 6-well plate using
613 Lipofectamine 3000 (Invitrogen). The cells were harvested 48 or 72 hours post transfection. To

614 establish an HFT cell line stably expressing doxycycline inducible FLAG-AGAL, 1 μg FLAG-AGAL
615 construct and 4.5 μg pOG44 was transfected into HFTs seeded onto a 6-well plate using
616 Lipofectamine 2000 (Invitrogen). After 48 hours the transfected cells were selected with
617 hygromycin (200 μg/mL) for about 10 days.

618 Cell pellets were lysed in either radioimmunoprecipitation assay (RIPA) buffer (25 mM
619 Tris-Cl [pH 7.6], 150 mM NaCl, 1 % NP-40, 1 % sodium deoxycholate, 0.1 % SDS, HALT protease
620 inhibitors (Pierce PI-78425), sodium vanadate, sodium fluoride) or in 1 % SDS lysis buffer (1 %
621 SDS, 50 mM Tris-Cl, 150 mM NaCl, 0.5 % NP-40, HALT protease inhibitors, sodium vanadate,
622 sodium fluoride). FLAG-AGAL and HA-PrP cell pellets were resuspended in RIPA buffer and
623 incubated on ice for 20 minutes with a 10 second vortex pulse every 5 minutes. Lysates were
624 then centrifuged at 14,000 rpm for 15 minutes at 4 °C. For UPR induction studies in Figure 1, cell
625 pellets were resuspended in SDS lysis buffer, vortexed briefly, boiled for 10 minutes at 95 °C, and
626 briefly vortexed. Lysates were incubated at 65 °C for an additional 5 minutes before centrifugation
627 at 14,000 rpm at room temperature. The supernatant was collected, and protein concentration
628 was estimated utilizing the DCA protein assay kit (Biorad). Protein expression was analyzed by
629 SDS-PAGE and immunoblot.

630 For immunoprecipitations, cell pellets were lysed in mammalian cell lysis buffer (50 mM
631 Tris-HCl [pH 7.6], 150 mM NaCl, 1 % Nonidet P-40, HALT protease inhibitors (Pierce), and 1 mM
632 DTT). Protein G agarose beads (Thermo Scientific 20398) was pre-washed with MCLB before
633 addition of the cell lysate and antibody (UBXN1, Sec61β, or rabbit IgG control). Samples were
634 incubated with rotation overnight at 4 °C. Beads was collected by centrifugation at 3000 rpm for
635 1 minute and was washed four times with MCLB buffer. Beads were resuspended in 50 μl SDS
636 sample buffer, briefly boiled, and processed for SDS-PAGE and immunoblotting.

637

638 **Antibodies, siRNA, and reagents**

639 The rabbit UBXN1 (16135-1-AP 1:7000 dilution), p97 (10736-1-AP), BAG6 (26417-1-AP), ATF6
640 (24169-1-AP), Sec61β (51020-2-AP 1:3000 dilution), Aconitase 2 (11134-1-AP), calnexin (10427-
641 2-AP), CYC1 (10242-1-AP), and G3BP1 (13057-2-AP) antibodies were obtained from Proteintech
642 Inc; rabbit BiP (3177 dilution), peIF2α (3398 1:500 dilution), and MCM3 (4012S) antibodies were
643 obtained from Cell Signaling Technology; mouse PCNA (sc-56 1:3000 dilution), ATF4 (sc-390063
644 1:500 dilution), Tom20 (sc-17764), ubiquitin (P4D1; sc8017), β-actin (sc-69879 1:3000 dilution),
645 GAPDH (sc-47724 1:3000 dilution), c-myc (sc-40 1:3000 dilution), Sec61α (sc-393182 1:500
646 dilution), and TRAPα (sc-373916) were from Santa Cruz Biotechnology; mouse ubiquitin FK2 (04-
647 263 1:100 dilution) for immunofluorescence and Anti-Puromycin, clone 12D10 (MABE343 1:3000
648 dilution) was from EMD Millipore; mouse FLAG-M2 antibody (F3165 1:1000 dilution) was from
649 Sigma Aldrich. The rabbit anti-Prion protein PrP antibody (ab52604) was purchased from Abcam.
650 The rabbit ALPP/ALPP2 was purchased from St. John's Laboratory (STJ96740). The mouse
651 HSP90AB1 was purchased from Origene (TA500494). All antibodies were used at a dilution of
652 1:1000 unless otherwise specified. Secondary antibodies, HRP conjugated anti-rabbit (W4011)
653 and anti-mouse (W4021) were from Promega and used at a dilution of 1:10000. Thapsigargin
654 (5860051MG), Tunicamycin (ICN15002801), Proteinase K (FEREO0491), and Hoechst (51-17
655 1:10000 dilution) for immunofluorescence were purchased from Fisher Scientific. Dithiothreitol
656 (DTT25) and puromycin (P-600-100) were purchased from GoldBio. Cyclohexmide (97064-724)
657 and Triton X-100 (97063-864) was purchased from VWR. CB-5083 were purchased from Cayman
658 Chemical Company (19311). Bortezomib (S1013) was purchased from Selleckchem. EndoH
659 (P0702S) was purchased from New England Biolabs. Crystal violet was purchased from Sigma-
660 Aldrich (C6158-50G). Doxycycline was purchased from EMD Millipore (324385-1GM). Wild-type
661 PrP (HA) was generously gifted by Ramanujan Hegde (MRC, UK). FLAG-tagged AGAL were
662 generously gifted by Malaiyalam Mariappan[66]. siRNAs against UBXN1-2 (D-008652-02), UBXN1-
663 3 (D-008652-03), and UBXN1-4 (D-008652-04) were purchased from Dharmacon. siRNA against

664 BAG6 (s15467) was purchased from Ambion (Themo Fisher Scientific). siControl (SIC001) was
665 from Millipore Sigma. siRNA against p97 was purchase from Invitrogen (HSS111263).
666
667 **Generation of CRISPR gene knockout cell lines**
668 UBXN1 knockout cells were generated in both HFT and HEK-293T cells using the CRISPR-Cas9
669 gene editing method. The guide sequence 5′-GCCGTCCCAGGATATGTCCAA-3′ was cloned into
670 the pX459 vector carrying hSpCas9 as previously published[40]. 500 ng of the construct was
671 transiently transfected into HFT and HEK-293T cells seeded in a 6-well plate with Lipofectamine
672 3000. 36 hours post-transfection, the cells were cultured with 1 μg/mL puromycin for an additional
673 24 hours. The surviving cells were counted and serially diluted to a concentration of 1 cell per well
674 in a 96-well plate. Protein expression of UBXN1 was examined by immunoblot.
675
676 **Crystal violet cell viability assay**
677 Wildtype and UBXN1 KO cells were plated at a density of 8000 cells/well in a 12-well dish. The
678 next day, cells were treated with 200 nM thapsigargin for the indicated timepoints. After treatment,
679 wells were washed twice with PBS before re-addition of fresh media. Every day for three days,
680 cells were washed once with PBS and media was replaced. On the third day, cells were washed
681 twice with PBS before incubation with 0.5 % crystal violet staining solution for 20 minutes at room
682 temperature on an orbital shaker. After staining, wells were washed thrice with PBS to remove
683 unbound stain. 1 % SDS-solution was added to each well to solubilize bound stain and the plate
684 was incubated for one hour at room temperature on an orbital shaker until color was uniform in
685 solution. The absorbance was read at 570 nm on a multiwell plate reader (SpectraMax iD3). The
686 average absorbance of wells without cells was used to background subtract.
687
688 **Real-time PCR**

689 For all real-time PCR experiments, total RNA was isolated using the *Quick*-RNA Miniprep Kit
690 (Zymo Research cat. no. R1055). The purified RNA was quantified by NanoDrop and 1 µg of RNA
691 for each sample was used to generate cDNA using the iScript cDNA synthesis kit (Biorad cat. no.
692 1708890). Real-time PCR was performed with PowerUp SYBR Green Master Mix (Applied
693 Biosystems cat. no. A25741) on an Applied Biosystems StepOnePlus real-time PCR system. Data
694 analyses utilized the $2^{-\Delta\Delta Ct}$ method and GAPDH was used as a housekeeping gene to normalize
695 transcript expression across samples. The XBP1s primers were previously published[52].
696
697 XBP1s forward: 5′ TGCTGAGTCCGCAGCAGGTG 3′
698 XBP1s reverse: 5′ GCTGGCAGGCTCTGGGGAAG 3′
699 Total XBP1 forward: 5′ AAACAGAGTAGCTCAGACTGC 3′
700 Total XBP1 reverse: 5′ TCCTTCTGGGTAGACCTCTGGGAG 3′
701 HA-PrP forward: 5’ CAGCCTCATGGTGGTGGCTG 3’
702 HA-PrP Reverse: 5’ GTCGGTCTCGGTGAAGTTCTCC 3’
703
704 **RT^2 Profiler PCR array**
705 Wildtype or UBXN1 KO HeLa Flp-in T-REX cells were grown in 10cm tissue culture dishes and
706 either left untreated or treated with 1.5 mM DTT for 4 hours. Post-harvest, RNA was extracted
707 from each sample with the *Quick*-RNA MiniPrep Kit (Zymo Research cat. no. R1055) and cDNA
708 was generated with the RT^2 First Strand Kit (Qiagen cat no. 330401). Each Human Unfolded
709 Protein Response RT^2 Profiler PCR Array (cat no. 330231 PAHS-089ZA) plate consists of 84
710 UPR specific target genes as well as a panel of housekeeping genes and PCR efficiency controls.
711 Each sample was distributed to an individual plate for two biological replicates each. The
712 GeneGlobe Data Analysis Center was used to determine the fold change between samples. The
713 data were normalized by automatic selection from the housekeeping gene panel utilizing the
714 geometric mean. The untreated wildtype HFT samples were defined as the “control” sample for

715 the data set and used to calculate fold changes. Heatmap visualizations for PCR array data were
716 performed using the RStudio software (v2022.07.1 Build 554), including ggplot2 (v 3.3.5), circlize
717 (v0.4.14), ComplexHeatmap version 2.10.0, and InteractiveComplexHeatmap package to export
718 heatmap generated by ComplexHeatmap into an interactive Shiny app[84].
719

720 **Immunofluorescence and microscopy**

721 To assess aggresome formation, cells were grown on coverslips (12mm) in a 24-well plate treated
722 with 1 μM bortezomib (Btz), Tunicamycin (Tu), or Thapsigargin (Tg) for 8 hours or 1 μM Btz, 500
723 nM Tu, or 500nM Tg for 18 hours. Cells were washed briefly in phosphate-buffered saline (PBS)
724 and fixed with ice-cold methanol for 10 min at −20°C. Cells were washed in PBS then blocked in
725 2 % bovine serum albumin (BSA) with 0.3 % Triton X-100 in PBS for 1 hour. The coverslips were
726 incubated with the indicated antibodies in a humidified chamber overnight at 4 °C. Coverslips
727 were washed and incubated with the appropriate Alexa Fluor-conjugated secondary antibodies
728 (Molecular Probes) for 1 hour in the dark at room temperature. Cells were washed with PBS, and
729 nuclei were stained with Hoechst 33342 dye and mounted onto slides. All images were collected
730 using a Nikon A1R scan head with a spectral detector and resonant scanners on a Ti-E motorized
731 inverted microscope equipped with a 60× Plan Apo 1.4 NA objective lens. The indicated
732 fluorophores were excited with either a 405-nm, 488-nm or 594-nm laser line. Images were
733 analyzed by using FIJI (https://imagej.net/Fiji).
734

735 **IRE1α-GFP foci imaging and quantification**

736 Stable HFT wildtype cells expressing doxycycline inducible IRE1α-3xFLAG-6xHis-GFP (construct
737 a generous gift from Peter Walter, UCSF) were seeded onto a 6-well plate and reverse transfected
738 with an siControl or siUBXN1[51]. Next day, cells were trypsinized and seeded onto coverslips in a
739 12-well plate. 48 hours after siRNA transection, IRE1α-GFP was induced with 4 μg/mL

740 doxycycline for an additional 24 hours. Next day, cells were either left untreated or treated with
741 2.5 μM tunicamycin for 4 hours. Coverslips were briefly washed with phosphate-buffered saline
742 (PBS) and fixed with ice-cold methanol for 10 min at -20 ^{o}C. Coverslips were washed with PBS
743 and nuclei were stained with Hoechst 33342 dye and mounted on slides. Images were collected
744 using either a 405-nm or 488-nm laser. One hundred cells were counted by creating a cell mask
745 and utilizing the "Find Maxima" function in FIJI (https://imagej.net/Fiji).
746

747 **Subcellular fractionation of ER-derived microsomes**

748 HEK-293T cells were seeded into four 150 mm sterile tissue culture dishes. Cells were scraped
749 off the plate into PBS, centrifuged at 600 x *g* for 5 minutes at 4 ^{o}C, and resuspended in ice-cold
750 homogenization buffer (225 mM Mannitol, 75 mM Sucrose, 30 mM Tris [pH 7.4]). Cells were
751 homogenized with a Dounce homogenizer on ice. Every 150 passes of the homogenizer, cells
752 were centrifuged for 5 minutes at 600 x *g*, to remove non-lysed cells and nuclei. The integrity of
753 the homogenized cells was examined under a light microscope until 80-90 % cell lysis was
754 attained. The supernatant was collected as the post-nuclear supernatant (PNS) fraction. The
755 clarified lysate was centrifuged at 7000 x *g* for 10 min at 4 ^{o}C, isolating the supernatant including
756 ER-microsomes. The supernatant was collected, centrifuged at 20,000 x *g* for 30 mins at 4 ^{o}C to
757 clear lysosomal and plasma membrane fractions. The resulting supernatant was further
758 centrifuged at high speed, 100,000 x *g* for 1 hour in a swinging-bucket rotor SW-41 and Beckman
759 Coulter ultracentrifuge. This results in the isolation of pure ER-microsomes (pellet) and cytosolic
760 fraction (supernatant). PNS, cytosolic, and ER-microsomes were solubilized using 0.5 % (v/v)
761 SDS and protein concentrations were determined by DC protein assay. An equivalent amount of
762 ER-microsomes were used in the protease protection assay. Of four aliquots, one was left
763 untreated, one was incubated with 1 % (v/v) Triton X-100, and the other two were incubated with
764 10 μg/mL proteinase K with or without 1 % (v/v) Triton X-100. All samples are incubated at 37 ^{o}C

765 for 10 minutes before reaction termination with 2 mM phenylmethylsulfonyl fluoride (PMSF). 5X-
766 Laemmli sample buffer was added to each sample before SDS-PAGE and immunoblot.
767
768 **Puromycilation translation assay**
769 Protein synthesis was measured in HFT wildtype and UBXN1 KO cells utilizing the non-
770 radioactive SUnSET assay[74]. HFT wildtype or UBXN1 KO cells were seeded onto a 6-well plate
771 at 400 k cells /well to achieve 70-80 % confluence at the time of puromycin addition. Cells were
772 incubated with 1 μM puromycin with or without 100 μg/ml cycloheximide for 30 minutes in
773 complete medium. Samples treated with DTT or thapsigargin were pre-incubated with 1.5 mM
774 DTT for 1 hour or 1 μM thapsigargin for 30 minutes before co-treatment of 1 μM puromycin with
775 1.5 mM DTT for 30 minutes in complete medium. At the end of the incubation period, cells were
776 washed with ice-cold PBS and the plate was immediately placed on ice. Ice-cold RIPA buffer was
777 added to the wells and cells were gently scraped into the buffer using a cell scraper. Lysates were
778 placed on ice and vortexed for 10 seconds every 5 minutes for 30 minutes before centrifugation
779 at 12,000 rpm for 10 minutes at 4 ^{o}C. Protein concentration was estimated using the DC assay
780 (Bio-Rad). An equivalent amount of protein for each sample were resolved by SDS-PAGE and
781 probed with the anti-puromycin antibody, clone 12D10.
782
783 **Polysome profiling**
784 HEK-293T wildtype and UBXN1 KO cells were plated in a 150 mm dish and allowed to grow for
785 two days before polysome isolation. For p97 depletion experiments, HEK-293T cells were plated
786 in a 150 mm dish and forward transfected next day with siRNA against p97 or an siControl. 24
787 hours later the plate was split into two 150 mm dishes and the cells were grown for two additional
788 days. The day before profiling, sucrose gradients were prepared with fresh 15 % and 60 %
789 sucrose solutions using 1X low-salt buffer (5 mM Tris-HCl [pH 7.5], 2.5 mM $MgCl_2$, 1.5 mM KCl,
790 1 mM PMSF). To generate a continuous gradient, 5 mL of 60 % sucrose solution was placed at

791 the bottom of an ultra-clear Beckman Coulter centrifuge tube. 5 mL of 15 % sucrose solution was
792 layered on top and the gradient was inverted horizontally and left on its side at room temperature
793 for 3 hours. After 3 hours, the tube was brought back to its vertical position and stored at 4 ^{o}C
794 overnight. When cells reached about 70-80 % confluency, cells were either pre-treated with 2 mM
795 DTT for 60 minutes or left untreated. After treatment, cells were incubated with 100 ug/mL
796 cycloheximide at 37 ^{o}C for 15-20 minutes. Cells were then washed twice with ice cold PBS
797 supplemented with 100 ug/mL cycloheximide and 1 mM PMSF, scraped off the plate, and pelleted
798 at 200 x *g* for 5 minutes at 4 ^{o}C. Cells were washed once with ice cold PBS, pelleted, and
799 resuspended in 480 uL 1X low salt buffer supplemented with 100 ug/mL cycloheximide, 2 uM
800 DTT, 1 mM PMSF, and 1 mM HALT protease inhibitor cocktail. 60 units of RNaseOUT
801 Recombinant RNase Inhibitor (Invitrogen, 10777019) was added to each sample and vortexed
802 for 5 seconds. Triton X-100 and sodium deoxycholate was added to each sample to a final
803 concentration of 0.5 % and samples were vortexed for an additional 5 seconds. Samples were
804 kept on ice for 5 minutes before centrifugation at 16,000 x *g* for 7 minutes at 4 ^{o}C. Samples were
805 quantified at 260 nm in UV compatible plates on a multiwell plate reader. 20 units of each sample
806 was loaded onto the continuous sucrose gradient and spun at 24,200 rpm for 3 hours 30 minutes
807 using an SW-41 swing bucket rotor in a Beckman Coulter ultracentrifuge. After the spin, the
808 samples were run on a continuous UA-6 detector, density gradient fractionator system with peak
809 detection software. Values determined by the fraction collector were graphed on GraphPad Prism.
810

811 **TMT-based proteomics**

812 **Sample preparation, digestion, and tandem-mass tag (TMT) labeling**

813 The TMT-based proteomics was performed exactly as previously described[85]. Briefly, 100 μg
814 protein of each sample was obtained by cell lysis in lysis buffer (8 M Urea, 200 mM N-(2-
815 Hydroxyethyl)piperazine-N′-(3-propanesulfonic acid) (EPPS) pH 8.5) followed by reduction using
816 5 mM tris(2-carboxyethyl)phosphine (TCEP), alkylation with 14 mM iodoacetamide and quenched

817 using 5 mM dithiothreitol. The reduced and alkylated protein was precipitated using methanol and
818 chloroform. The protein mixture was digested with LysC (Wako) overnight followed by Trypsin
819 (Pierce) digestion for 6 hours at 37ºC. The trypsin was inactivated with 30% (v/v) acetonitrile. The
820 digested peptides were labelled with 0.2 mg per reaction of 4-plex TMT reagents (ThermoFisher
821 scientific) (126, 127N, 129N, and 129C) at room temperature for 1 hour. The reaction was
822 quenched using 0.5% (v/v) Hydroxylamine for 15 min. A 2.5 μL aliquot from the labeling reaction
823 was tested for labeling efficiency. TMT-labeled peptides from each sample were pooled together
824 at a 1:1 ratio. The pooled peptide mix was dried under vacuum and resuspended in 5% formic
825 acid for 15 min. The resuspended peptide sample was further purified using C18 solid-phase
826 extraction (SPE) (Sep-Pak, Waters).
827
828 **Off-line basic pH reverse-phase (BPRP) fractionation.**
829 We fractionated the pooled, labeled peptide sample using BPRP HPLC[86]. We used an Agilent
830 1200 pump equipped with a degasser and a detector (set at 220 and 280 nm wavelength).
831 Peptides were subjected to a 60-min linear gradient from 5% to 35% acetonitrile in 10 mM
832 ammonium bicarbonate pH 8 at a flow rate of 0.25 mL/min over an Agilent 300Extend C18 column
833 (3.5 µm particles, 2.1 mm ID and 250 mm in length). The peptide mixture was fractionated into a
834 total of 96 fractions, which were consolidated into 24 super-fractions[87]. Samples were
835 subsequently acidified with 1% formic acid and vacuum centrifuged to near dryness. Each
836 consolidated fraction was desalted via StageTip, dried again via vacuum centrifugation, and
837 reconstituted in 5% acetonitrile, 5% formic acid for LC-MS/MS processing.
838
839 **Liquid chromatography and tandem mass spectrometry**.
840 Mass spectrometric data were collected on an Orbitrap Fusion mass spectrometer coupled to a
841 Proxeon NanoLC-1000 UHPLC. The 100 µm capillary column was packed with 35 cm of Accucore

842 150 resin (2.6 µm, 150Å; ThermoFisher Scientific). The scan sequence began with an MS1
843 spectrum (Orbitrap analysis, resolution 120,000, 350−1400 Th, automatic gain control (AGC)
844 target 5 x10^5, maximum injection time 100 ms). Data were acquired for 150 minutes per fraction.
845 SPS-MS3 analysis was used to reduce ion interference[88,89]. MS2 analysis consisted of collision-
846 induced dissociation (CID), quadrupole ion trap analysis, automatic gain control (AGC) 1 x10^4,
847 NCE (normalized collision energy) 35, q-value 0.25, maximum injection time 60 ms), isolation
848 window at 0.7 Th. Following acquisition of each MS2 spectrum, we collected an MS3 spectrum in
849 which multiple MS2 fragment ions were captured in the MS3 precursor population using isolation
850 waveforms with multiple frequency notches. MS3 precursors were fragmented by HCD and
851 analyzed using the Orbitrap (NCE 65, AGC 2.0 x10^5, isolation window 1.3 Th, maximum injection
852 time 150 ms, resolution was 50,000).
853
854 **Data analysis.**
855 Spectra were converted to mzXML via MSconvert[90]. Database searching included all entries from
856 the Human UniProt Database (downloaded: April 2016). The database was concatenated with
857 one composed of all protein sequences for that database in the reversed order. Searches were
858 performed using a 50-ppm precursor ion tolerance for total protein level profiling. The product ion
859 tolerance was set to 0.9 Da. These wide mass tolerance windows were chosen to maximize
860 sensitivity in conjunction with Comet searches and linear discriminant analysis[91,92]. TMT tags on
861 lysine residues and peptide N-termini (+229.163 Da for TMT) and carbamidomethylation of
862 cysteine residues (+57.021 Da) were set as static modifications, while oxidation of methionine
863 residues (+15.995 Da) was set as a variable modification. Peptide-spectrum matches (PSMs)
864 were adjusted to a 1% false discovery rate (FDR)[93,94]. PSM filtering was performed using a linear
865 discriminant analysis, as described previously[92] and then assembled further to a final protein-
866 level FDR of 1% [94]. Proteins were quantified by summing reporter ion counts across all matching

867 PSMs, also as described previously[95]. Reporter ion intensities were adjusted to correct for the
868 isotopic impurities of the different TMT reagents according to manufacturer specifications. The
869 signal-to-noise (S/N) measurements of peptides assigned to each protein were summed and
870 these values were normalized so that the sum of the signal for all proteins in each channel was
871 equivalent to account for equal protein loading. Finally, each protein abundance measurement
872 was scaled, such that the summed signal-to-noise for that protein across all channels equaled
873 100, thereby generating a relative abundance (RA) measurement.
874 Downstream data analyses for TMT datasets were carried out using the R statistical package
875 (v4.0.3) and Bioconductor (v3.12; BiocManager 1.30.10). TMT channel intensities were quantile
876 normalized and then the data were log-transformed. The log transformed data were analyzed with
877 limma-based R package where p-values were FDR adjusted using an empirical Bayesian
878 statistical. Differentially expressed proteins were determined using a $\log_2$ (fold change (WT *vs*
879 UBXN1 KO)) threshold of > +/- 0.65.
880
881 **Gene ontology (GO) functional enrichment analyses of proteomics data.**
882 The differentially expressed proteins were further annotated and GO functional enrichment
883 analysis was performed using Metascape online tool (http://metascape.org)[96]. The GO cluster
884 network and protein-protein interaction network generated by metascape and the STRING
885 database (https://string-db.org/), respectively, were imported into Cytoscape software (v3.8.2) to
886 add required attributes (fold changes, p-values, gene number, and conditions) and prepared for
887 the visualization. Other proteomic data visualizations were performed using the RStudio software
888 (v1.4.1103), including hrbrthemes (v0.8.0), viridis (v0.6.1), dplyr (v.1.0.7), and ggplot2 (v 3.3.5).
889
890 **Quantification and statistical analysis**

Immunoblots were quantified using densitometry on FIJI and protein levels were normalized to the loading control for that experiment (GAPDH or β-actin). Fold changes, SEM, and statistical significance was calculated using GraphPad Prism (version 9.4). Statistical tests performed are indicated in figure legends and include unpaired two-tailed Student's *t*-test or one-way ANOVA with post-hoc analysis indicated in figure legends.

Acknowledgements

We thank Peter Juo and Michelle Johnson and Rakesh Ganji for critical reading of the manuscript. We are grateful to Peter Walter (University of California San Francisco and Altos Labs) for the GFP-IRE1 construct, and Mals Mariappan (Yale University) for the FLAG-AGAL construct. This work is supported by the NIH grants GM127557, NS123631 and a Research Scholar Grant RSG-19-022-01 from the American Cancer Society to M.R. This work was funded in part by NIH/NIGMS grant GM67945 (S.P.G.) and R01 GM132129 (J.A.P.).

Respective Contributions

B.A and M.R conceived the studies. R.G performed TMT proteomics and data analysis, S.M performed aggresome studies. J.P and S.P.G assisted with proteomic studies. B.A and M.R wrote the manuscript.

Competing Interests

The authors declare no conflicts of interest.

Request for reagents

Please contact the corresponding author, M.R for reagent requests.

916 **Data availability**

917 All raw proteomic data will be made available on public servers upon acceptance of the
918 manuscript. Any other data is available from the corresponding author upon request.

919

920 **REFERENCES**

921 1 Kaufman, R. J. Orchestrating the unfolded protein response in health and disease. *J Clin*
922 *Invest* **110**, 1389-1398, doi:10.1172/JCI16886 (2002).

923 2 Bellucci, A. *et al.* Induction of the unfolded protein response by alpha-synuclein in
924 experimental models of Parkinson's disease. *J Neurochem* **116**, 588-605,
925 doi:10.1111/j.1471-4159.2010.07143.x (2011).

926 3 Duennwald, M. L. & Lindquist, S. Impaired ERAD and ER stress are early and specific
927 events in polyglutamine toxicity. *Genes Dev* **22**, 3308-3319, doi:10.1101/gad.1673408
928 (2008).

929 4 Atkin, J. D. *et al.* Endoplasmic reticulum stress and induction of the unfolded protein
930 response in human sporadic amyotrophic lateral sclerosis. *Neurobiol Dis* **30**, 400-407,
931 doi:10.1016/j.nbd.2008.02.009 (2008).

932 5 Hoozemans, J. J. *et al.* The unfolded protein response is activated in pretangle neurons
933 in Alzheimer's disease hippocampus. *Am J Pathol* **174**, 1241-1251,
934 doi:10.2353/ajpath.2009.080814 (2009).

935 6 Nishitoh, H. *et al.* ALS-linked mutant SOD1 induces ER stress- and ASK1-dependent
936 motor neuron death by targeting Derlin-1. *Genes Dev* **22**, 1451-1464,
937 doi:10.1101/gad.1640108 (2008).

938 7 Cooper, A. A. *et al.* Alpha-synuclein blocks ER-Golgi traffic and Rab1 rescues neuron loss
939 in Parkinson's models. *Science* **313**, 324-328, doi:10.1126/science.1129462 (2006).

940 8 Yang, H. *et al.* Huntingtin interacts with the cue domain of gp78 and inhibits gp78 binding
941 to ubiquitin and p97/VCP. *PLoS One* **5**, e8905, doi:10.1371/journal.pone.0008905 (2010).

942 9 Vonk, W. I. M. *et al.* Differentiation Drives Widespread Rewiring of the Neural Stem Cell
943 Chaperone Network. *Mol Cell* **78**, 329-345 e329, doi:10.1016/j.molcel.2020.03.009
944 (2020).
945 10 Brehme, M. *et al.* A chaperome subnetwork safeguards proteostasis in aging and
946 neurodegenerative disease. *Cell Rep* **9**, 1135-1150, doi:10.1016/j.celrep.2014.09.042
947 (2014).
948 11 Rousseau, A. & Bertolotti, A. An evolutionarily conserved pathway controls proteasome
949 homeostasis. *Nature* **536**, 184-189, doi:10.1038/nature18943 (2016).
950 12 Shoulders, M. D. *et al.* Stress-independent activation of XBP1s and/or ATF6 reveals three
951 functionally diverse ER proteostasis environments. *Cell Rep* **3**, 1279-1292,
952 doi:10.1016/j.celrep.2013.03.024 (2013).
953 13 Bertolotti, A., Zhang, Y., Hendershot, L. M., Harding, H. P. & Ron, D. Dynamic interaction
954 of BiP and ER stress transducers in the unfolded-protein response. *Nat Cell Biol* **2**, 326-
955 332, doi:10.1038/35014014 (2000).
956 14 Kopp, M. C., Larburu, N., Durairaj, V., Adams, C. J. & Ali, M. M. U. UPR proteins IRE1
957 and PERK switch BiP from chaperone to ER stress sensor. *Nat Struct Mol Biol* **26**, 1053-
958 1062, doi:10.1038/s41594-019-0324-9 (2019).
959 15 Pincus, D. *et al.* BiP binding to the ER-stress sensor Ire1 tunes the homeostatic behavior
960 of the unfolded protein response. *PLoS Biol* **8**, e1000415,
961 doi:10.1371/journal.pbio.1000415 (2010).
962 16 Harding, H. P., Zhang, Y., Bertolotti, A., Zeng, H. & Ron, D. Perk is essential for
963 translational regulation and cell survival during the unfolded protein response. *Mol Cell* **5**,
964 897-904, doi:10.1016/s1097-2765(00)80330-5 (2000).
965 17 Calfon, M. *et al.* IRE1 couples endoplasmic reticulum load to secretory capacity by
966 processing the XBP-1 mRNA. *Nature* **415**, 92-96, doi:10.1038/415092a (2002).

967 18 Yoshida, H., Matsui, T., Yamamoto, A., Okada, T. & Mori, K. XBP1 mRNA is induced by
968 ATF6 and spliced by IRE1 in response to ER stress to produce a highly active transcription
969 factor. *Cell* **107**, 881-891, doi:10.1016/s0092-8674(01)00611-0 (2001).
970 19 Hollien, J. *et al.* Regulated Ire1-dependent decay of messenger RNAs in mammalian cells.
971 *J Cell Biol* **186**, 323-331, doi:10.1083/jcb.200903014 (2009).
972 20 Lipson, K. L., Ghosh, R. & Urano, F. The role of IRE1alpha in the degradation of insulin
973 mRNA in pancreatic beta-cells. *PLoS One* **3**, e1648, doi:10.1371/journal.pone.0001648
974 (2008).
975 21 Oikawa, D., Tokuda, M. & Iwawaki, T. Site-specific cleavage of CD59 mRNA by
976 endoplasmic reticulum-localized ribonuclease, IRE1. *Biochem Biophys Res Commun* **360**,
977 122-127, doi:10.1016/j.bbrc.2007.06.020 (2007).
978 22 Ghosh, A. P., Klocke, B. J., Ballestas, M. E. & Roth, K. A. CHOP potentially co-operates
979 with FOXO3a in neuronal cells to regulate PUMA and BIM expression in response to ER
980 stress. *PLoS One* **7**, e39586, doi:10.1371/journal.pone.0039586 (2012).
981 23 Urano, F. *et al.* Coupling of stress in the ER to activation of JNK protein kinases by
982 transmembrane protein kinase IRE1. *Science* **287**, 664-666,
983 doi:10.1126/science.287.5453.664 (2000).
984 24 Kato, H. *et al.* mTORC1 serves ER stress-triggered apoptosis via selective activation of
985 the IRE1-JNK pathway. *Cell Death Differ* **19**, 310-320, doi:10.1038/cdd.2011.98 (2012).
986 25 Twomey, E. C. *et al.* Substrate processing by the Cdc48 ATPase complex is initiated by
987 ubiquitin unfolding. *Science* **365**, doi:10.1126/science.aax1033 (2019).
988 26 Pan, M. *et al.* Mechanistic insight into substrate processing and allosteric inhibition of
989 human p97. *Nat Struct Mol Biol* **28**, 614-625, doi:10.1038/s41594-021-00617-2 (2021).
990 27 Bodnar, N. O. & Rapoport, T. A. Molecular Mechanism of Substrate Processing by the
991 Cdc48 ATPase Complex. *Cell* **169**, 722-735 e729, doi:10.1016/j.cell.2017.04.020 (2017).

992 28 Meyer, H. & Weihl, C. C. The VCP/p97 system at a glance: connecting cellular function to
993 disease pathogenesis. *J Cell Sci* **127**, 3877-3883, doi:10.1242/jcs.093831 (2014).
994 29 Ye, Y., Meyer, H. H. & Rapoport, T. A. Function of the p97-Ufd1-Npl4 complex in
995 retrotranslocation from the ER to the cytosol: dual recognition of nonubiquitinated
996 polypeptide segments and polyubiquitin chains. *J Cell Biol* **162**, 71-84,
997 doi:10.1083/jcb.200302169 (2003).
998 30 Raman, M. *et al.* Systematic proteomics of the VCP-UBXD adaptor network identifies a
999 role for UBXN10 in regulating ciliogenesis. *Nat Cell Biol* **17**, 1356-1369,
1000 doi:10.1038/ncb3238 (2015).
1001 31 Buchberger, A., Schindelin, H. & Hanzelmann, P. Control of p97 function by cofactor
1002 binding. *FEBS Lett* **589**, 2578-2589, doi:10.1016/j.febslet.2015.08.028 (2015).
1003 32 Zhang, X. *et al.* Altered cofactor regulation with disease-associated p97/VCP mutations.
1004 *Proc Natl Acad Sci U S A* **112**, E1705-1714, doi:10.1073/pnas.1418820112 (2015).
1005 33 Weihl, C. C., Dalal, S., Pestronk, A. & Hanson, P. I. Inclusion body myopathy-associated
1006 mutations in p97/VCP impair endoplasmic reticulum-associated degradation. *Hum Mol*
1007 *Genet* **15**, 189-199, doi:10.1093/hmg/ddi426 (2006).
1008 34 Watts, G. D. *et al.* Inclusion body myopathy associated with Paget disease of bone and
1009 frontotemporal dementia is caused by mutant valosin-containing protein. *Nat Genet* **36**,
1010 377-381, doi:10.1038/ng1332 (2004).
1011 35 Schroder, R. *et al.* Mutant valosin-containing protein causes a novel type of frontotemporal
1012 dementia. *Ann Neurol* **57**, 457-461, doi:10.1002/ana.20407 (2005).
1013 36 Tang, W. K. & Xia, D. Mutations in the Human AAA(+) Chaperone p97 and Related
1014 Diseases. *Front Mol Biosci* **3**, 79, doi:10.3389/fmolb.2016.00079 (2016).
1015 37 Gonzalez, M. A. *et al.* A novel mutation in VCP causes Charcot-Marie-Tooth Type 2
1016 disease. *Brain* **137**, 2897-2902, doi:10.1093/brain/awu224 (2014).

1017 38 Gonzalez-Perez, P. *et al.* Novel mutation in VCP gene causes atypical amyotrophic lateral
1018 sclerosis. *Neurology* **79**, 2201-2208, doi:10.1212/WNL.0b013e318275963b (2012).
1019 39 Chan, N. *et al.* Valosin-containing protein mutation and Parkinson's disease. *Parkinsonism*
1020 *Relat Disord* **18**, 107-109, doi:10.1016/j.parkreldis.2011.07.006 (2012).
1021 40 Ganji, R., Mukkavalli, S., Somanji, F. & Raman, M. The VCP-UBXN1 Complex Mediates
1022 Triage of Ubiquitylated Cytosolic Proteins Bound to the BAG6 Complex. *Mol Cell Biol* **38**,
1023 doi:10.1128/MCB.00154-18 (2018).
1024 41 Hegde, R. S. & Keenan, R. J. Tail-anchored membrane protein insertion into the
1025 endoplasmic reticulum. *Nat Rev Mol Cell Biol* **12**, 787-798, doi:10.1038/nrm3226 (2011).
1026 42 Hegde, R. S. & Zavodszky, E. Recognition and Degradation of Mislocalized Proteins in
1027 Health and Disease. *Cold Spring Harb Perspect Biol* **11**,
1028 doi:10.1101/cshperspect.a033902 (2019).
1029 43 Guna, A. & Hegde, R. S. Transmembrane Domain Recognition during Membrane Protein
1030 Biogenesis and Quality Control. *Curr Biol* **28**, R498-R511, doi:10.1016/j.cub.2018.02.004
1031 (2018).
1032 44 Rodrigo-Brenni, M. C., Gutierrez, E. & Hegde, R. S. Cytosolic quality control of
1033 mislocalized proteins requires RNF126 recruitment to Bag6. *Mol Cell* **55**, 227-237,
1034 doi:10.1016/j.molcel.2014.05.025 (2014).
1035 45 Mariappan, M. *et al.* A ribosome-associating factor chaperones tail-anchored membrane
1036 proteins. *Nature* **466**, 1120-1124, doi:10.1038/nature09296 (2010).
1037 46 Wang, Q. *et al.* A ubiquitin ligase-associated chaperone holdase maintains polypeptides
1038 in soluble states for proteasome degradation. *Mol Cell* **42**, 758-770,
1039 doi:10.1016/j.molcel.2011.05.010 (2011).
1040 47 Ernst, R. *et al.* Enzymatic blockade of the ubiquitin-proteasome pathway. *PLoS Biol* **8**,
1041 e1000605, doi:10.1371/journal.pbio.1000605 (2011).

1042 48 Claessen, J. H. & Ploegh, H. L. BAT3 guides misfolded glycoproteins out of the
1043 endoplasmic reticulum. *PLoS One* **6**, e28542, doi:10.1371/journal.pone.0028542 (2011).
1044 49 Hong, M., Li, M., Mao, C. & Lee, A. S. Endoplasmic reticulum stress triggers an acute
1045 proteasome-dependent degradation of ATF6. *J Cell Biochem* **92**, 723-732,
1046 doi:10.1002/jcb.20118 (2004).
1047 50 Belyy, V., Tran, N. H. & Walter, P. Quantitative microscopy reveals dynamics and fate of
1048 clustered IRE1alpha. *Proc Natl Acad Sci U S A* **117**, 1533-1542,
1049 doi:10.1073/pnas.1915311117 (2020).
1050 51 Li, H., Korennykh, A. V., Behrman, S. L. & Walter, P. Mammalian endoplasmic reticulum
1051 stress sensor IRE1 signals by dynamic clustering. *Proc Natl Acad Sci U S A* **107**, 16113-
1052 16118, doi:10.1073/pnas.1010580107 (2010).
1053 52 van Schadewijk, A., van't Wout, E. F., Stolk, J. & Hiemstra, P. S. A quantitative method
1054 for detection of spliced X-box binding protein-1 (XBP1) mRNA as a measure of
1055 endoplasmic reticulum (ER) stress. *Cell Stress Chaperones* **17**, 275-279,
1056 doi:10.1007/s12192-011-0306-2 (2012).
1057 53 LaLonde, D. P. & Bretscher, A. The UBX protein SAKS1 negatively regulates endoplasmic
1058 reticulum-associated degradation and p97-dependent degradation. *J Biol Chem* **286**,
1059 4892-4901, doi:10.1074/jbc.M110.158030 (2011).
1060 54 Mukkavalli, S., Klickstein, J. A., Ortiz, B., Juo, P. & Raman, M. The p97-UBXN1 complex
1061 regulates aggresome formation. *J Cell Sci* **134**, doi:10.1242/jcs.254201 (2021).
1062 55 Okada, T., Yoshida, H., Akazawa, R., Negishi, M. & Mori, K. Distinct roles of activating
1063 transcription factor 6 (ATF6) and double-stranded RNA-activated protein kinase-like
1064 endoplasmic reticulum kinase (PERK) in transcription during the mammalian unfolded
1065 protein response. *Biochem J* **366**, 585-594, doi:10.1042/BJ20020391 (2002).

1066 56 Gonen, N., Sabath, N., Burge, C. B. & Shalgi, R. Widespread PERK-dependent repression
1067 of ER targets in response to ER stress. *Sci Rep* **9**, 4330, doi:10.1038/s41598-019-38705-
1068 5 (2019).
1069 57 Shinjo, S., Mizotani, Y., Tashiro, E. & Imoto, M. Comparative analysis of the expression
1070 patterns of UPR-target genes caused by UPR-inducing compounds. *Biosci Biotechnol*
1071 *Biochem* **77**, 729-735, doi:10.1271/bbb.120812 (2013).
1072 58 Travers, K. J. *et al.* Functional and genomic analyses reveal an essential coordination
1073 between the unfolded protein response and ER-associated degradation. *Cell* **101**, 249-
1074 258, doi:10.1016/s0092-8674(00)80835-1 (2000).
1075 59 Harding, H. P. *et al.* An integrated stress response regulates amino acid metabolism and
1076 resistance to oxidative stress. *Mol Cell* **11**, 619-633, doi:10.1016/s1097-2765(03)00105-9
1077 (2003).
1078 60 Han, J. *et al.* ER-stress-induced transcriptional regulation increases protein synthesis
1079 leading to cell death. *Nat Cell Biol* **15**, 481-490, doi:10.1038/ncb2738 (2013).
1080 61 Guan, B. J. *et al.* Translational control during endoplasmic reticulum stress beyond
1081 phosphorylation of the translation initiation factor eIF2alpha. *J Biol Chem* **289**, 12593-
1082 12611, doi:10.1074/jbc.M113.543215 (2014).
1083 62 Krokowski, D. *et al.* A self-defeating anabolic program leads to beta-cell apoptosis in
1084 endoplasmic reticulum stress-induced diabetes via regulation of amino acid flux. *J Biol*
1085 *Chem* **288**, 17202-17213, doi:10.1074/jbc.M113.466920 (2013).
1086 63 Ye, Y. *et al.* Recruitment of the p97 ATPase and ubiquitin ligases to the site of
1087 retrotranslocation at the endoplasmic reticulum membrane. *Proc Natl Acad Sci U S A* **102**,
1088 14132-14138, doi:10.1073/pnas.0505006102 (2005).
1089 64 Ye, Y., Shibata, Y., Yun, C., Ron, D. & Rapoport, T. A. A membrane protein complex
1090 mediates retro-translocation from the ER lumen into the cytosol. *Nature* **429**, 841-847,
1091 doi:10.1038/nature02656 (2004).

1092 65 Wang, L. *et al.* TMUB1 is an endoplasmic reticulum-resident escortase that promotes the
1093 p97-mediated extraction of membrane proteins for degradation. *Mol Cell* **82**, 3453-3467
1094 e3414, doi:10.1016/j.molcel.2022.07.006 (2022).
1095 66 Sun, S., Li, X. & Mariappan, M. Signal sequences encode information for protein folding
1096 in the endoplasmic reticulum. *J Cell Biol* **222**, doi:10.1083/jcb.202203070 (2023).
1097 67 Kang, S. W. *et al.* Substrate-specific translocational attenuation during ER stress defines
1098 a pre-emptive quality control pathway. *Cell* **127**, 999-1013, doi:10.1016/j.cell.2006.10.032
1099 (2006).
1100 68 Hori, O. *et al.* Transmission of cell stress from endoplasmic reticulum to mitochondria:
1101 enhanced expression of Lon protease. *J Cell Biol* **157**, 1151-1160,
1102 doi:10.1083/jcb.200108103 (2002).
1103 69 Bravo, R. *et al.* Increased ER-mitochondrial coupling promotes mitochondrial respiration
1104 and bioenergetics during early phases of ER stress. *J Cell Sci* **124**, 2143-2152,
1105 doi:10.1242/jcs.080762 (2011).
1106 70 Rainbolt, T. K., Atanassova, N., Genereux, J. C. & Wiseman, R. L. Stress-regulated
1107 translational attenuation adapts mitochondrial protein import through Tim17A degradation.
1108 *Cell Metab* **18**, 908-919, doi:10.1016/j.cmet.2013.11.006 (2013).
1109 71 Schmidt, E. K., Clavarino, G., Ceppi, M. & Pierre, P. SUnSET, a nonradioactive method
1110 to monitor protein synthesis. *Nat Methods* **6**, 275-277, doi:10.1038/nmeth.1314 (2009).
1111 72 Yarmolinsky, M. B. & Haba, G. L. Inhibition by Puromycin of Amino Acid Incorporation into
1112 Protein. *Proc Natl Acad Sci U S A* **45**, 1721-1729, doi:10.1073/pnas.45.12.1721 (1959).
1113 73 Nathans, D. Puromycin Inhibition of Protein Synthesis: Incorporation of Puromycin into
1114 Peptide Chains. *Proc Natl Acad Sci U S A* **51**, 585-592, doi:10.1073/pnas.51.4.585 (1964).
1115 74 Ravi, V., Jain, A., Mishra, S. & Sundaresan, N. R. Measuring Protein Synthesis in Cultured
1116 Cells and Mouse Tissues Using the Non-radioactive SUnSET Assay. *Curr Protoc Mol Biol*
1117 **133**, e127, doi:10.1002/cpmb.127 (2020).

1118 75 Kim, J. Y. *et al.* ER Stress Drives Lipogenesis and Steatohepatitis via Caspase-2
1119 Activation of S1P. *Cell* **175**, 133-145 e115, doi:10.1016/j.cell.2018.08.020 (2018).
1120 76 Okada, K. *et al.* Prolonged endoplasmic reticulum stress in hypertrophic and failing heart
1121 after aortic constriction: possible contribution of endoplasmic reticulum stress to cardiac
1122 myocyte apoptosis. *Circulation* **110**, 705-712, doi:10.1161/01.CIR.0000137836.95625.D4
1123 (2004).
1124 77 Ljubkovic, M. *et al.* Disturbed Fatty Acid Oxidation, Endoplasmic Reticulum Stress, and
1125 Apoptosis in Left Ventricle of Patients With Type 2 Diabetes. *Diabetes* **68**, 1924-1933,
1126 doi:10.2337/db19-0423 (2019).
1127 78 Ramalingam, L., Sopontammarak, B., Menikdiwela, K. R. & Moustaid-Moussa, N.
1128 Endoplasmic Reticulum (ER) Stress in Part Mediates Effects of Angiotensin II in
1129 Pancreatic Beta Cells. *Diabetes Metab Syndr Obes* **13**, 2843-2853,
1130 doi:10.2147/DMSO.S257797 (2020).
1131 79 Kawai, T. *et al.* IPS-1, an adaptor triggering RIG-I- and Mda5-mediated type I interferon
1132 induction. *Nat Immunol* **6**, 981-988, doi:10.1038/ni1243 (2005).
1133 80 Wang, P. *et al.* UBXN1 interferes with Rig-I-like receptor-mediated antiviral immune
1134 response by targeting MAVS. *Cell Rep* **3**, 1057-1070, doi:10.1016/j.celrep.2013.02.027
1135 (2013).
1136 81 Hu, Y. *et al.* Multiple UBXN family members inhibit retrovirus and lentivirus production and
1137 canonical NFkappaBeta signaling by stabilizing IkappaBalpha. *PLoS Pathog* **13**,
1138 e1006187, doi:10.1371/journal.ppat.1006187 (2017).
1139 82 Walczak, C. P. *et al.* Ribosomal protein RPL26 is the principal target of UFMylation. *Proc*
1140 *Natl Acad Sci U S A* **116**, 1299-1308, doi:10.1073/pnas.1816202116 (2019).
1141 83 Wang, L. *et al.* UFMylation of RPL26 links translocation-associated quality control to
1142 endoplasmic reticulum protein homeostasis. *Cell Res* **30**, 5-20, doi:10.1038/s41422-019-
1143 0236-6 (2020).

1144 84 Gu, Z., Eils, R. & Schlesner, M. Complex heatmaps reveal patterns and correlations in
1145 multidimensional genomic data. *Bioinformatics* **32**, 2847-2849,
1146 doi:10.1093/bioinformatics/btw313 (2016).
1147 85 Ganji, R. *et al.* The p97-UBXD8 complex modulates ER-Mitochondria contact sites by
1148 modulating membrane lipid saturation and composition. *bioRxiv*, 2021.2012.2008.471763,
1149 doi:10.1101/2021.12.08.471763 (2021).
1150 86 Wang, Y. *et al.* Reversed-phase chromatography with multiple fraction concatenation
1151 strategy for proteome profiling of human MCF10A cells. *Proteomics* **11**, 2019-2026,
1152 doi:10.1002/pmic.201000722 (2011).
1153 87 Paulo, J. A. *et al.* Quantitative mass spectrometry-based multiplexing compares the
1154 abundance of 5000 S. cerevisiae proteins across 10 carbon sources. *J Proteomics* **148**,
1155 85-93, doi:10.1016/j.jprot.2016.07.005 (2016).
1156 88 Gygi, J. P. *et al.* Web-Based Search Tool for Visualizing Instrument Performance Using
1157 the Triple Knockout (TKO) Proteome Standard. *J Proteome Res* **18**, 687-693,
1158 doi:10.1021/acs.jproteome.8b00737 (2019).
1159 89 Paulo, J. A., O'Connell, J. D. & Gygi, S. P. A Triple Knockout (TKO) Proteomics Standard
1160 for Diagnosing Ion Interference in Isobaric Labeling Experiments. *J Am Soc Mass*
1161 *Spectrom* **27**, 1620-1625, doi:10.1007/s13361-016-1434-9 (2016).
1162 90 Chambers, M. C. *et al.* A cross-platform toolkit for mass spectrometry and proteomics. *Nat*
1163 *Biotechnol* **30**, 918-920, doi:10.1038/nbt.2377 (2012).
1164 91 Beausoleil, S. A., Villen, J., Gerber, S. A., Rush, J. & Gygi, S. P. A probability-based
1165 approach for high-throughput protein phosphorylation analysis and site localization.
1166 *Nature biotechnology* **24**, 1285-1292, doi:10.1038/nbt1240 (2006).
1167 92 Huttlin, E. L. *et al.* A tissue-specific atlas of mouse protein phosphorylation and
1168 expression. *Cell* **143**, 1174-1189, doi:10.1016/j.cell.2010.12.001 (2010).

1169 93 Elias, J. E. & Gygi, S. P. Target-decoy search strategy for mass spectrometry-based
1170 proteomics. *Methods Mol Biol* **604**, 55-71, doi:10.1007/978-1-60761-444-9_5 (2010).
1171 94 Elias, J. E. & Gygi, S. P. Target-decoy search strategy for increased confidence in large-
1172 scale protein identifications by mass spectrometry. *Nat Methods* **4**, 207-214,
1173 doi:10.1038/nmeth1019 (2007).
1174 95 McAlister, G. C. *et al.* Increasing the Multiplexing Capacity of TMTs Using Reporter Ion
1175 Isotopologues with Isobaric Masses. *Analytical Chemistry* **84**, 7469-7478,
1176 doi:10.1021/ac301572t (2012).
1177 96 Zhou, Y. *et al.* Metascape provides a biologist-oriented resource for the analysis of
1178 systems-level datasets. *Nat Commun* **10**, 1523, doi:10.1038/s41467-019-09234-6 (2019).
1179

Figure 1

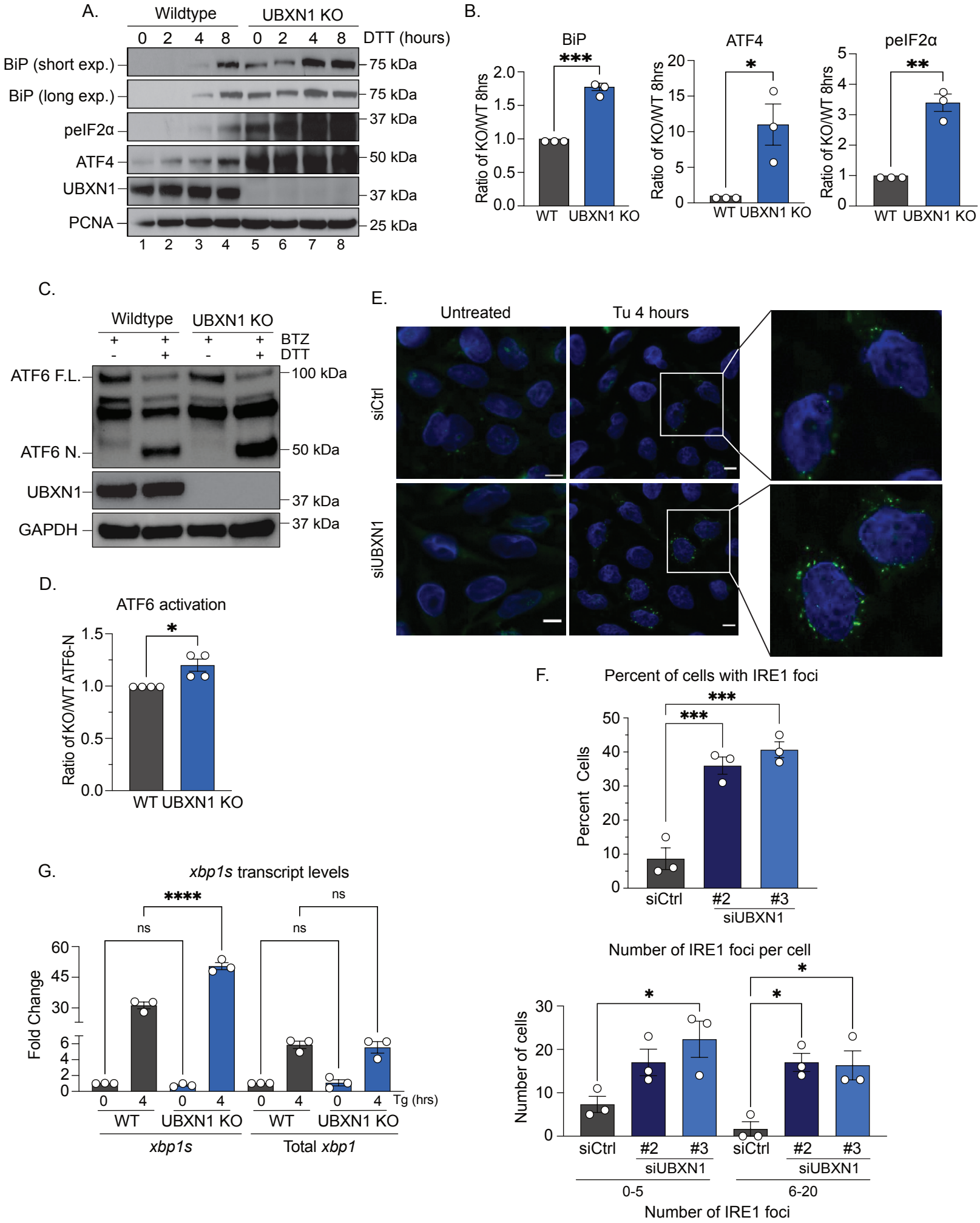
A.
Wildtype
UBXN1 KO
0 2 4 8 0 2 4 8
DTT (hours)
BiP (short exp.)
BiP (long exp.)
peIF2α
ATF4
UBXN1
PCNA
75 kDa
75 kDa
37 kDa
50 kDa
37 kDa
25 kDa
1 2 3 4 5 6 7 8
B.
BiP
ATF4
peIF2α
Ratio of KO/WT 8hrs
WT UBXN1 KO
C.
Wildtype
UBXN1 KO
BTZ
DTT
ATF6 F.L.
ATF6 N.
UBXN1
GAPDH
100 kDa
50 kDa
37 kDa
37 kDa
D.
ATF6 activation
Ratio of KO/WT ATF6-N
WT UBXN1 KO
E.
Untreated
Tu 4 hours
siCtrl
siUBXN1
F.
Percent of cells with IRE1 foci
Percent Cells
siCtrl
#2
#3
siUBXN1
Number of IRE1 foci per cell
Number of cells
0-5
6-20
Number of IRE1 foci
G.
xbp1s transcript levels
Fold Change
ns
Tg (hrs)
WT UBXN1 KO
xbp1s
Total xbp1

Figure 2

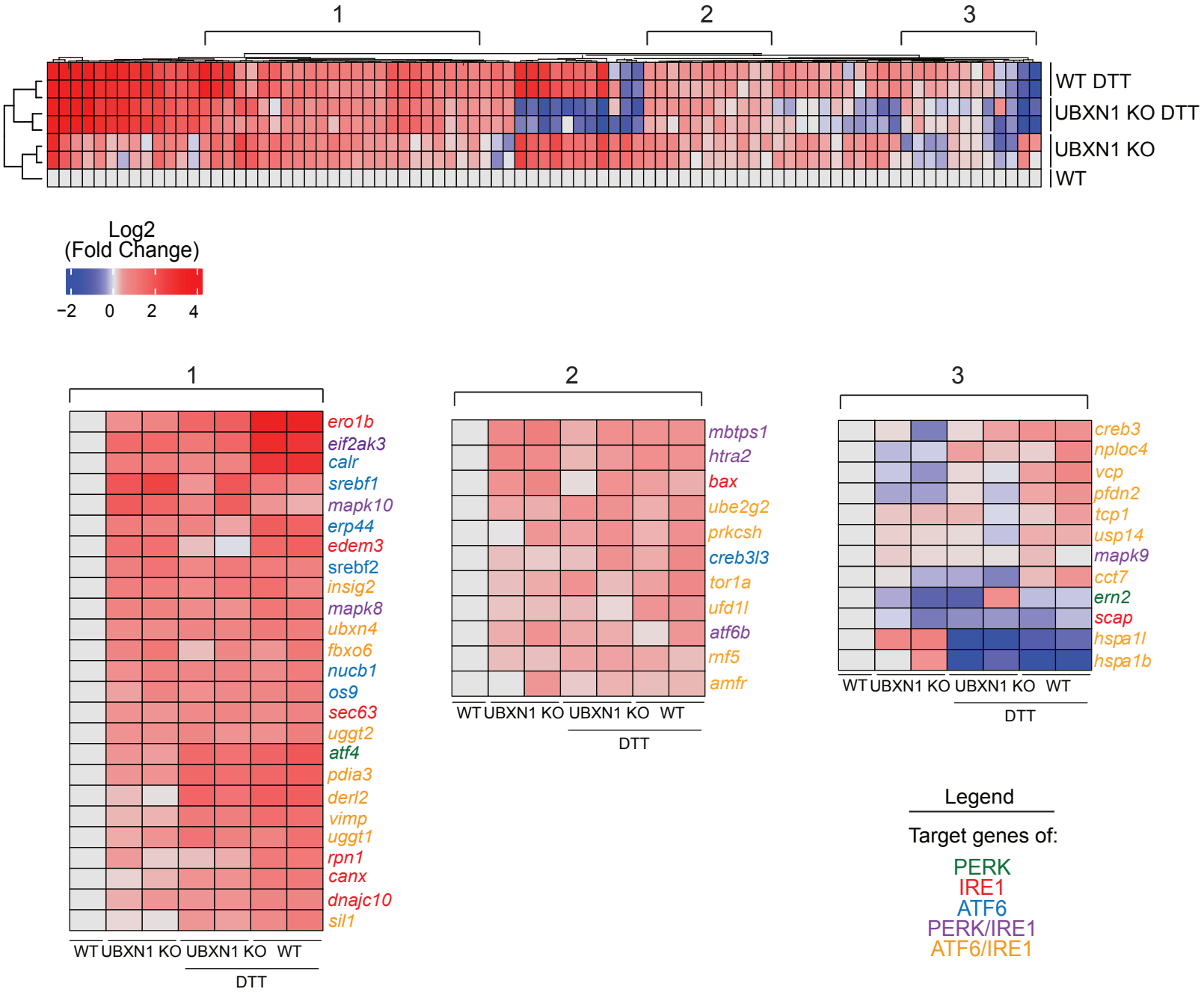
1
2
3
WT DTT
UBXN1 KO DTT
UBXN1 KO
WT
Log2
(Fold Change)
−2
0
2
4
ero1b
eif2ak3
calr
srebf1
mapk10
erp44
edem3
srebf2
insig2
mapk8
ubxn4
fbxo6
nucb1
os9
sec63
uggt2
atf4
pdia3
derl2
vimp
uggt1
rpn1
canx
dnajc10
sil1
WT UBXN1 KO UBXN1 KO WT
DTT
mbtps1
htra2
bax
ube2g2
prkcsh
creb3l3
tor1a
ufd1l
atf6b
rnf5
amfr
WT UBXN1 KO UBXN1 KO WT
DTT
creb3
nploc4
vcp
pfdn2
tcp1
usp14
mapk9
cct7
ern2
scap
hspa1l
hspa1b
WT UBXN1 KO UBXN1 KO WT
DTT
Legend
Target genes of:
PERK
IRE1
ATF6
PERK/IRE1
ATF6/IRE1

Figure 3

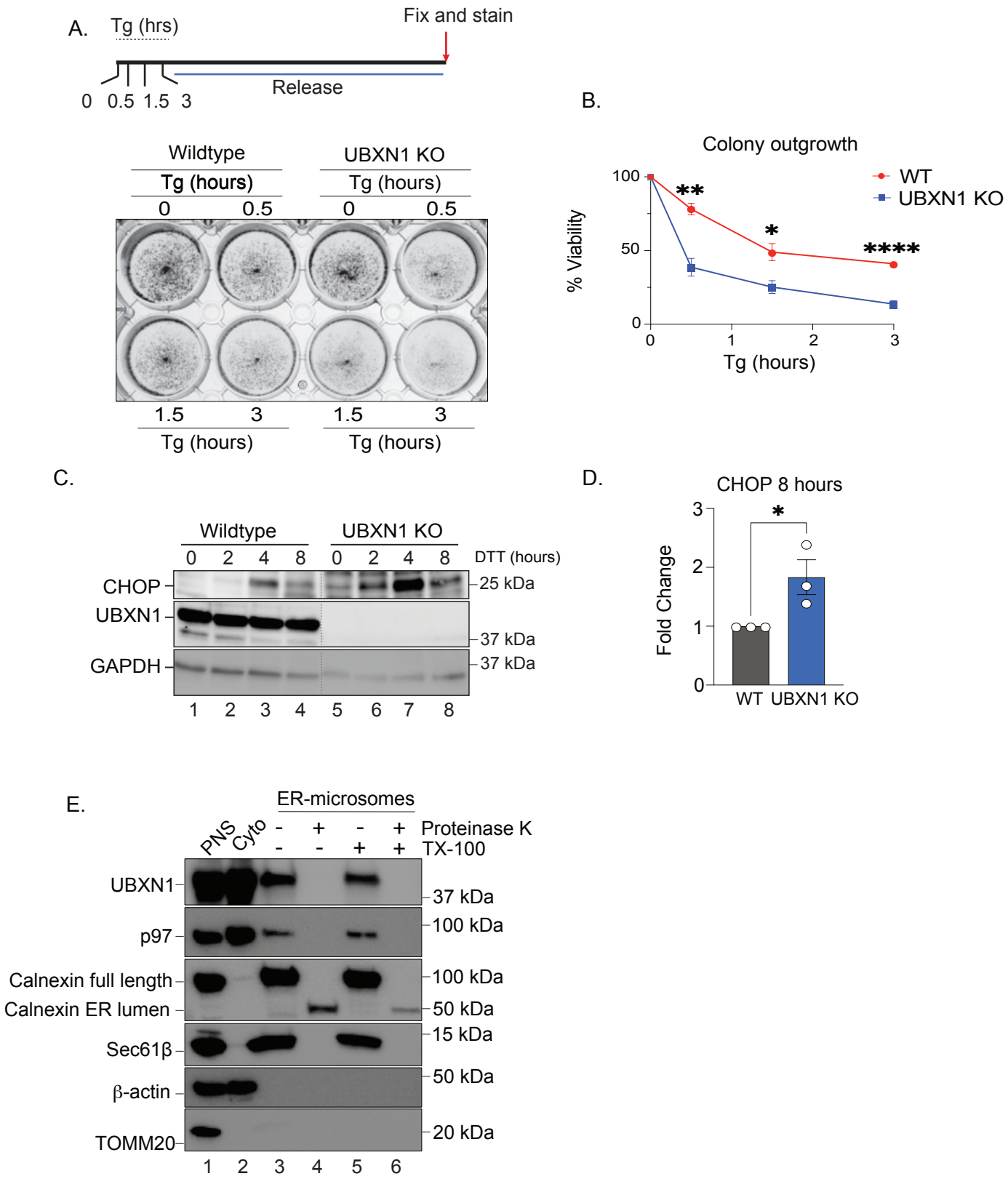
A.
Tg (hrs)
Fix and stain
Release
0 0.5 1.5 3
Wildtype
UBXN1 KO
Tg (hours)
0 0.5 0 0.5
1.5 3 1.5 3
Tg (hours)
B.
Colony outgrowth
WT
UBXN1 KO
% Viability
Tg (hours)
C.
Wildtype
UBXN1 KO
0 2 4 8 0 2 4 8
DTT (hours)
CHOP
UBXN1
GAPDH
25 kDa
37 kDa
37 kDa
1 2 3 4 5 6 7 8
D.
CHOP 8 hours
Fold Change
WT UBXN1 KO
E.
ER-microsomes
PNS Cyto
Proteinase K
TX-100
UBXN1
p97
Calnexin full length
Calnexin ER lumen
Sec61β
β-actin
TOMM20
37 kDa
100 kDa
100 kDa
50 kDa
15 kDa
50 kDa
20 kDa
1 2 3 4 5 6

Figure 4

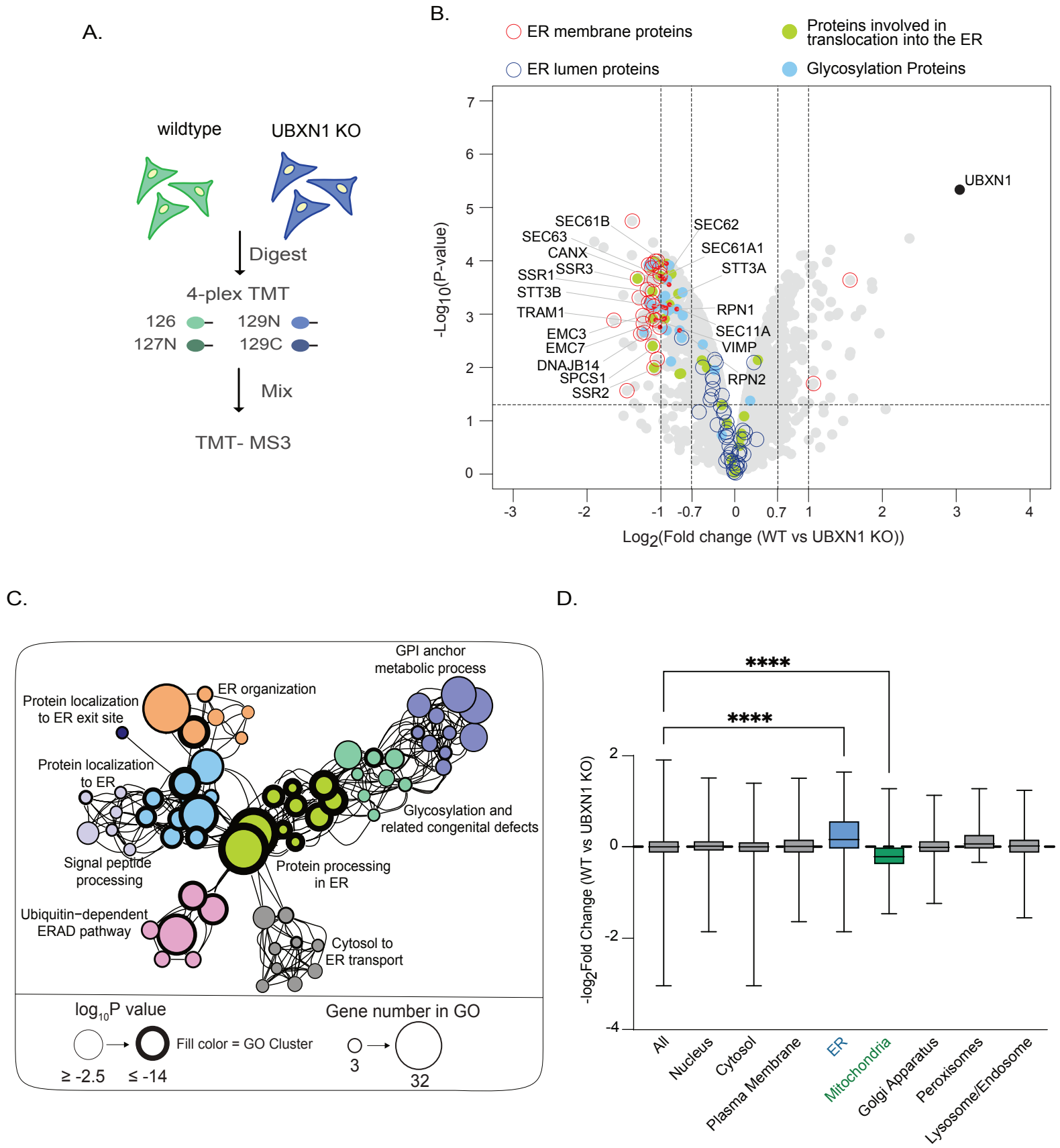
A.
wildtype
UBXN1 KO
Digest
4-plex TMT
126
127N
129N
129C
Mix
TMT- MS3
B.
ER membrane proteins
ER lumen proteins
Proteins involved in translocation into the ER
Glycosylation Proteins
UBXN1
SEC61B
SEC63
CANX
SSR3
SSR1
STT3B
TRAM1
EMC3
EMC7
DNAJB14
SPCS1
SSR2
SEC62
SEC61A1
STT3A
RPN1
SEC11A
VIMP
RPN2
-Log10(P-value)
Log2(Fold change (WT vs UBXN1 KO))
C.
GPI anchor metabolic process
ER organization
Protein localization to ER exit site
Protein localization to ER
Glycosylation and related congenital defects
Signal peptide processing
Protein processing in ER
Ubiquitin−dependent ERAD pathway
Cytosol to ER transport
log10P value
≥ -2.5
≤ -14
Fill color = GO Cluster
Gene number in GO
3
32
D.
****
****
-log2Fold Change (WT vs UBXN1 KO)
All
Nucleus
Cytosol
Plasma Membrane
ER
Mitochondria
Golgi Apparatus
Peroxisomes
Lysosome/Endosome

Figure 5

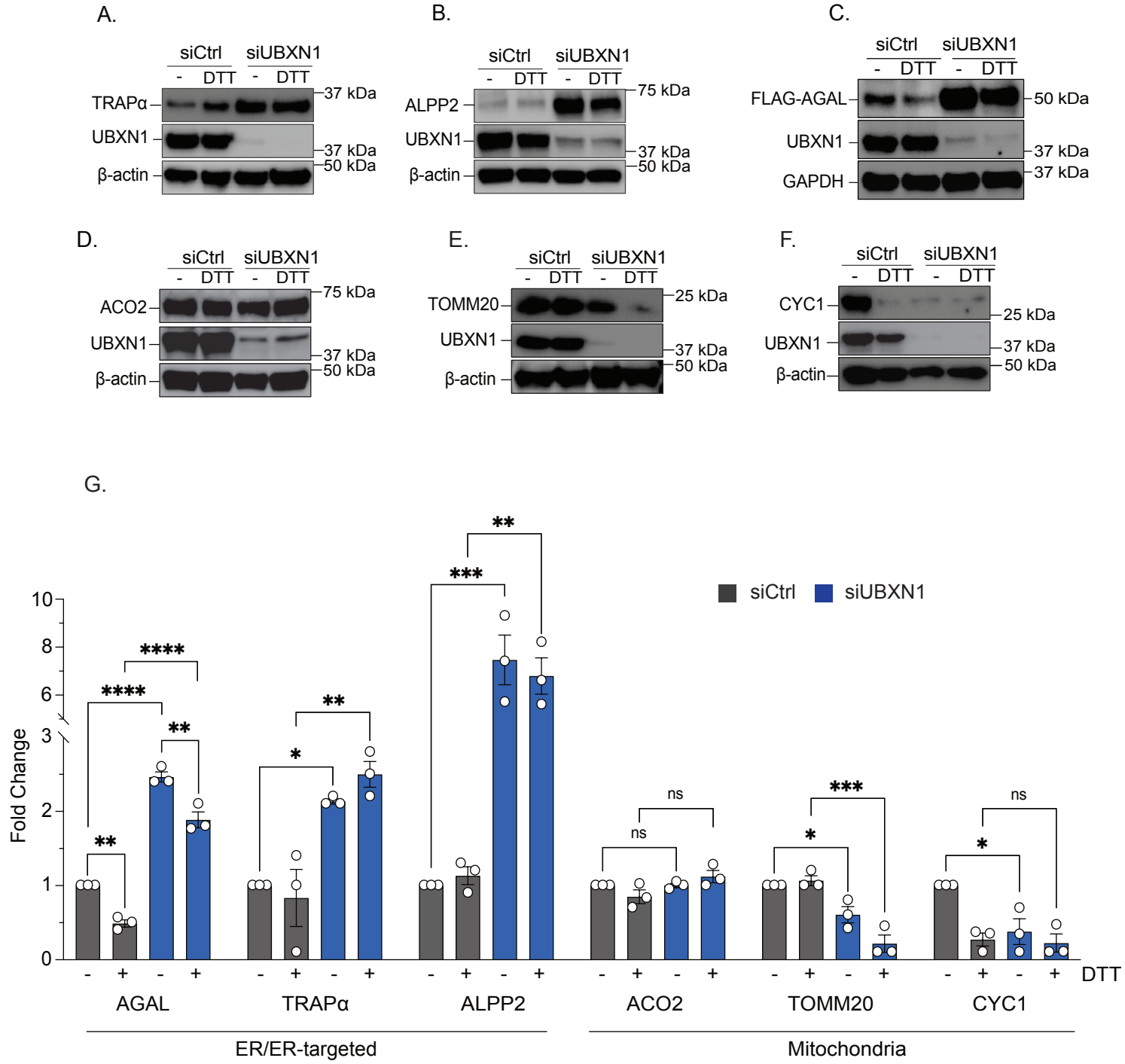
A.
siCtrl
siUBXN1
- DTT - DTT
TRAPα
UBXN1
β-actin
37 kDa
37 kDa
50 kDa
B.
siCtrl
siUBXN1
- DTT - DTT
ALPP2
UBXN1
β-actin
75 kDa
37 kDa
50 kDa
C.
siCtrl
siUBXN1
- DTT - DTT
FLAG-AGAL
UBXN1
GAPDH
50 kDa
37 kDa
37 kDa
D.
siCtrl
siUBXN1
- DTT - DTT
ACO2
UBXN1
β-actin
75 kDa
37 kDa
50 kDa
E.
siCtrl
siUBXN1
- DTT - DTT
TOMM20
UBXN1
β-actin
25 kDa
37 kDa
50 kDa
F.
siCtrl
siUBXN1
- DTT - DTT
CYC1
UBXN1
β-actin
25 kDa
37 kDa
50 kDa
G.
siCtrl
siUBXN1
Fold Change
10
8
6
3
2
1
0
****
****
**
**
*
**
***
**
ns
ns
***
*
ns
*
- + - + - + - + - + - + - + - + - + - + - + - + DTT
AGAL
TRAPα
ALPP2
ACO2
TOMM20
CYC1
ER/ER-targeted
Mitochondria

Figure 6

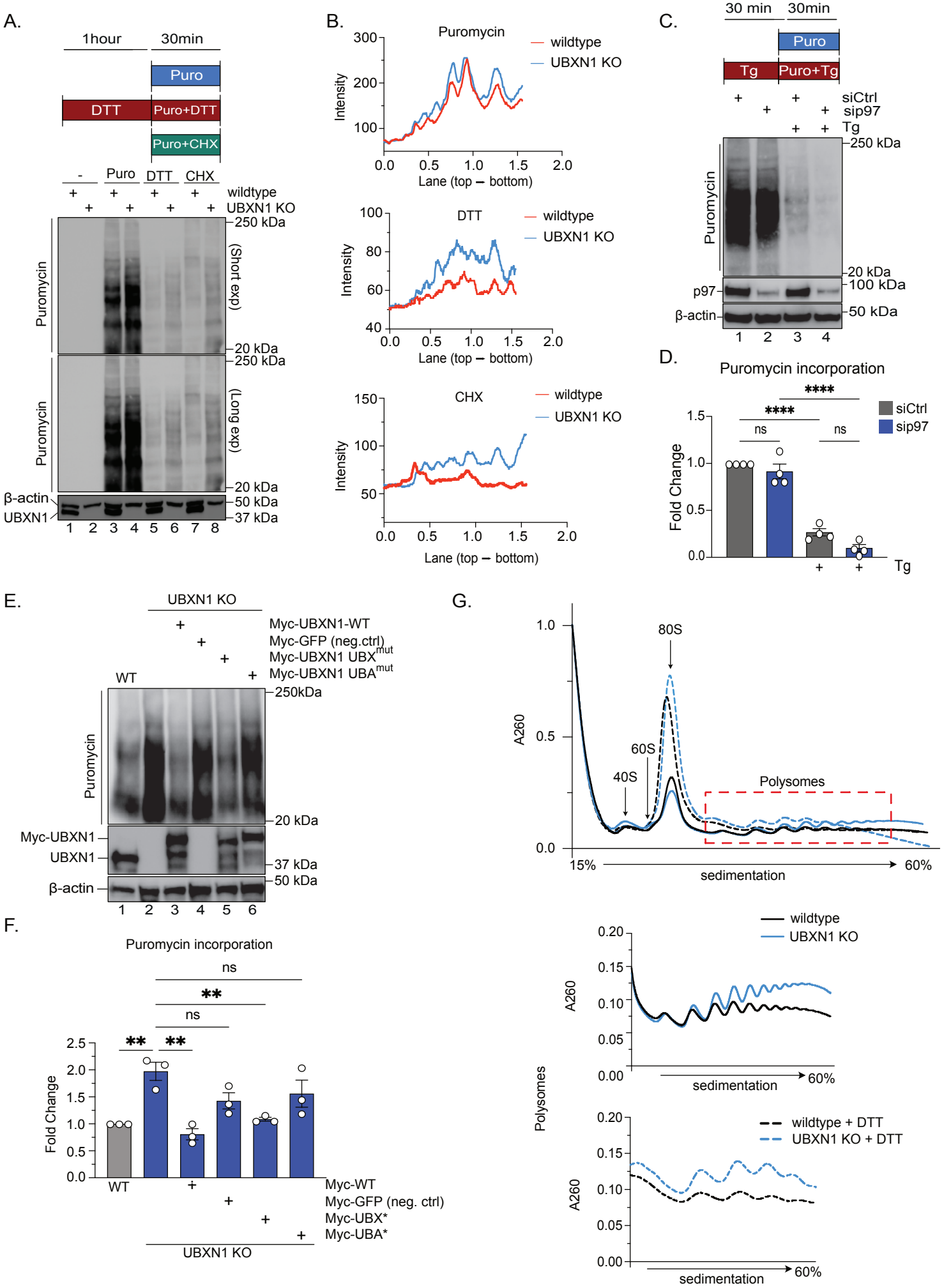
A.
1hour
30min
Puro
DTT
Puro+DTT
Puro+CHX
-
Puro
DTT
CHX
wildtype
UBXN1 KO
250 kDa
Puromycin
(Short exp)
20 kDa
250 kDa
Puromycin
(Long exp)
20 kDa
β-actin
50 kDa
UBXN1
37 kDa
1 2 3 4 5 6 7 8
B.
Puromycin
wildtype
UBXN1 KO
Intensity
Lane (top → bottom)
DTT
CHX
C.
30 min
30min
Puro
Tg
Puro+Tg
siCtrl
sip97
Tg
250 kDa
Puromycin
20 kDa
p97
100 kDa
β-actin
50 kDa
1 2 3 4
D.
Puromycin incorporation
siCtrl
sip97
Fold Change
ns
****
Tg
E.
UBXN1 KO
Myc-UBXN1-WT
Myc-GFP (neg.ctrl)
Myc-UBXN1 UBX^mut
Myc-UBXN1 UBA^mut
WT
250kDa
Puromycin
20 kDa
Myc-UBXN1
UBXN1
37 kDa
β-actin
50 kDa
1 2 3 4 5 6
G.
80S
60S
40S
Polysomes
A260
15%
60%
sedimentation
wildtype
UBXN1 KO
wildtype + DTT
UBXN1 KO + DTT
F.
Puromycin incorporation
ns
**
Fold Change
WT
Myc-WT
Myc-GFP (neg. ctrl)
Myc-UBX*
Myc-UBA*
UBXN1 KO

Figure 7

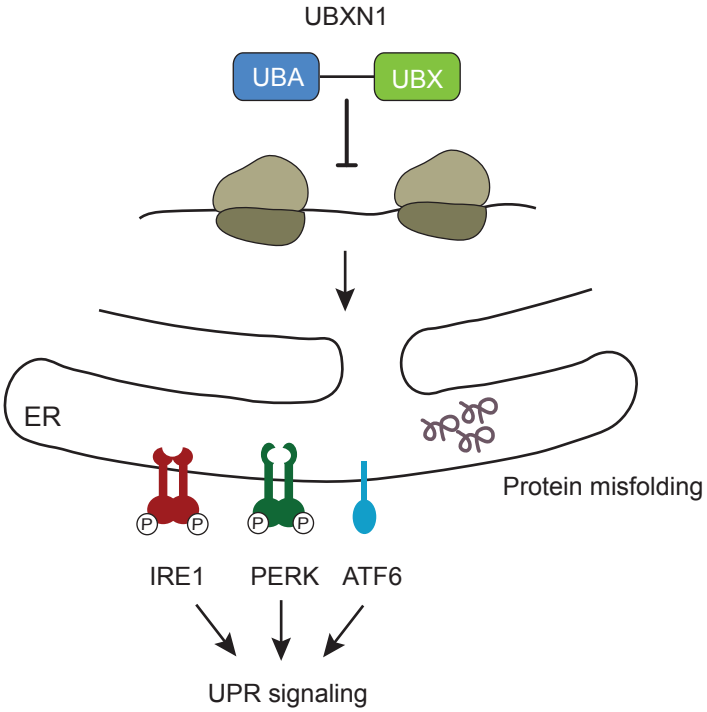
UBXN1
UBA
UBX
ER
Protein misfolding
P
P
P
P
IRE1
PERK
ATF6
UPR signaling

Supplementary Figure 1

A.

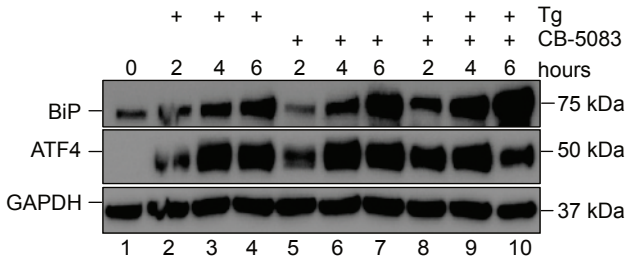

B.

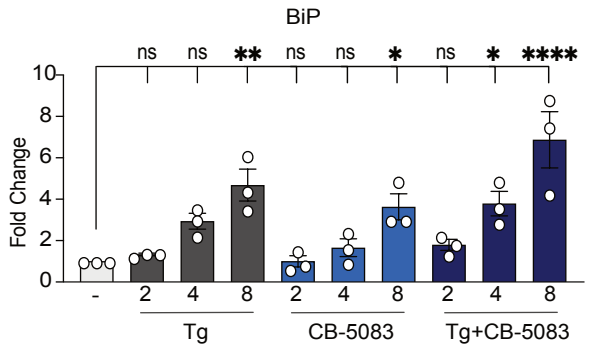

C.

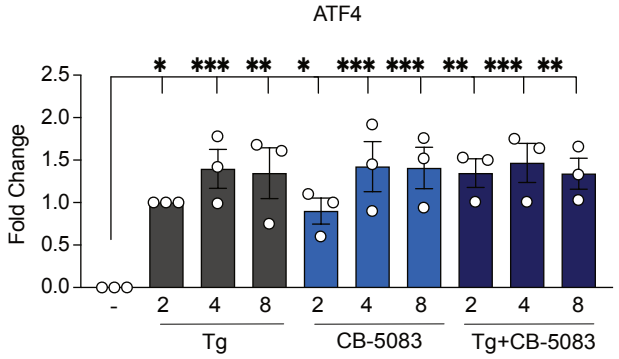

D.

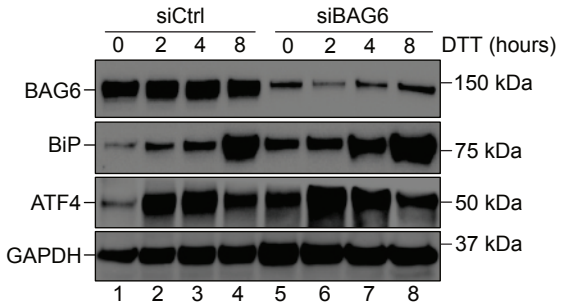

E.

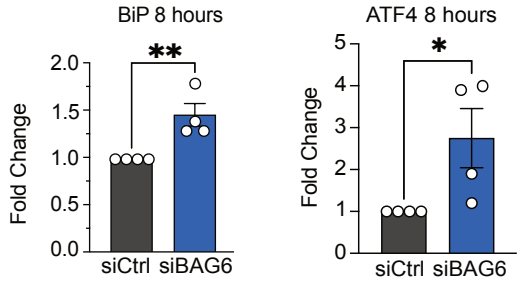

F.

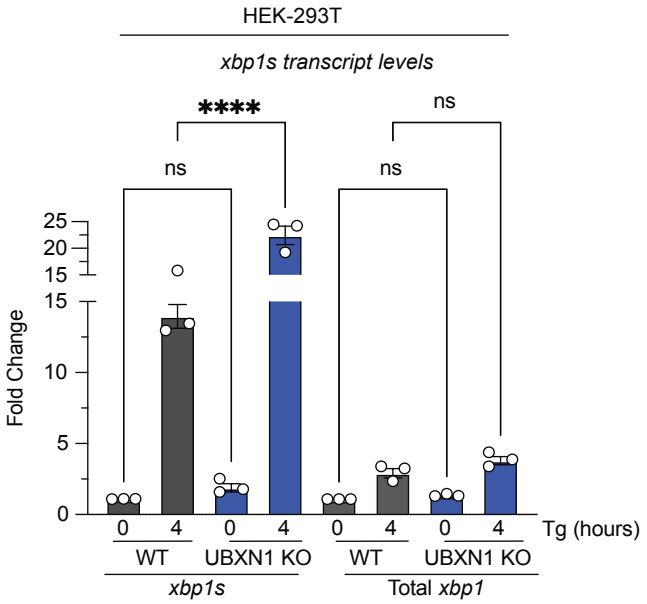

G.

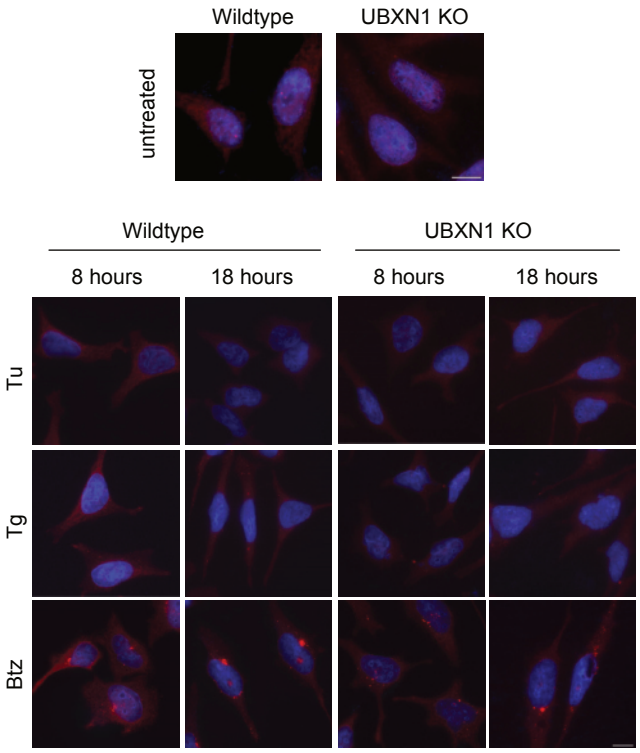

H.

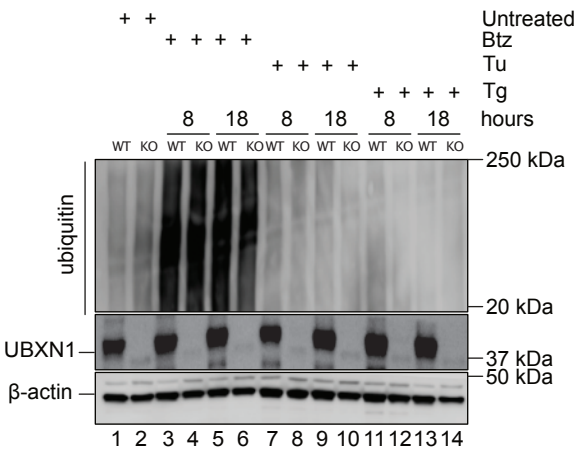

Supplementary Figure 2

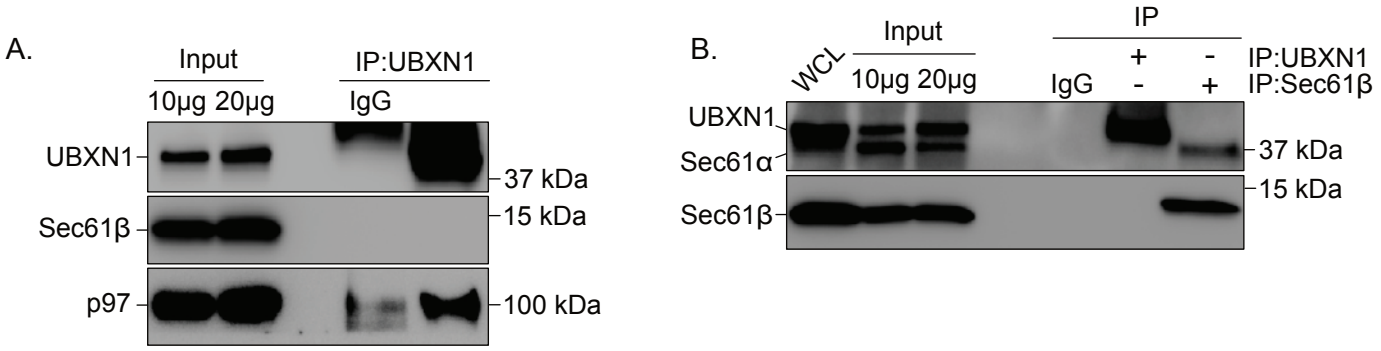

Supplementary Figure 3

A.

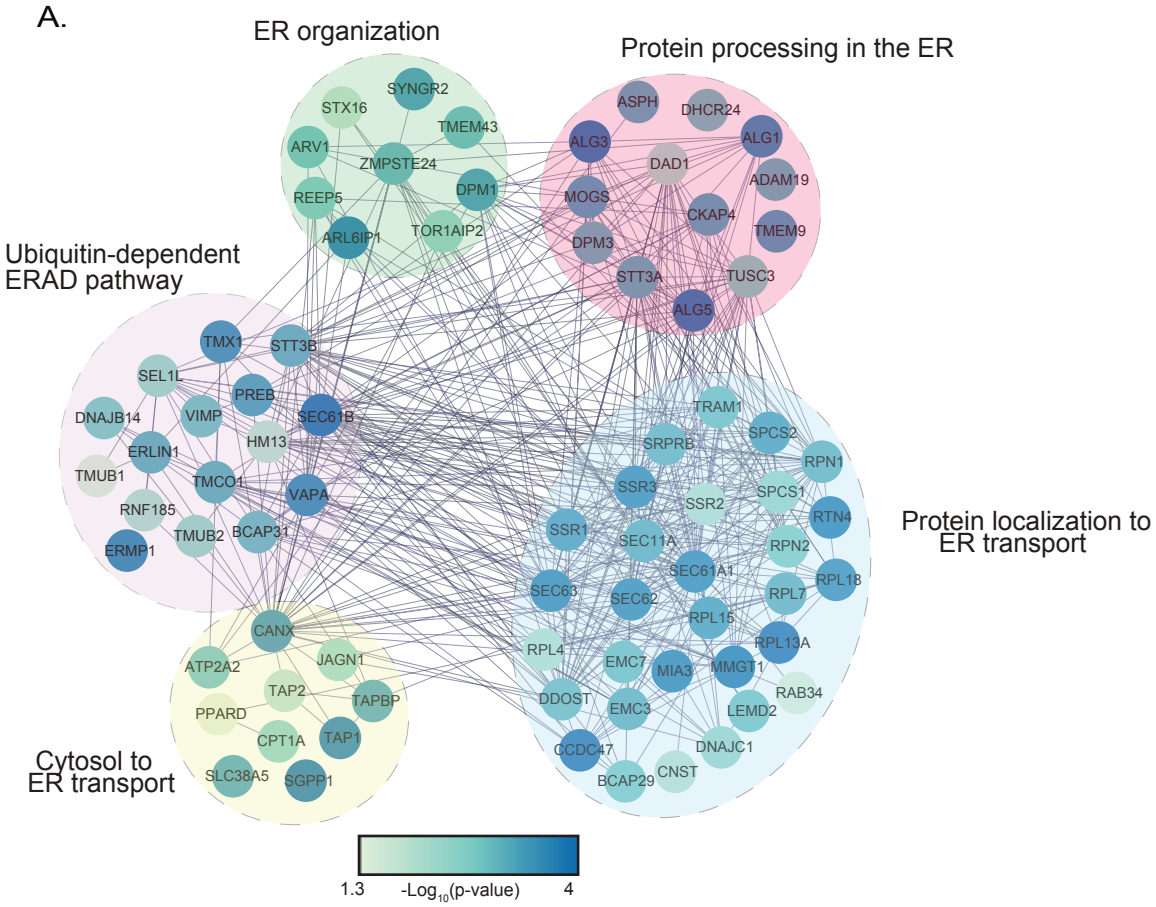

B.

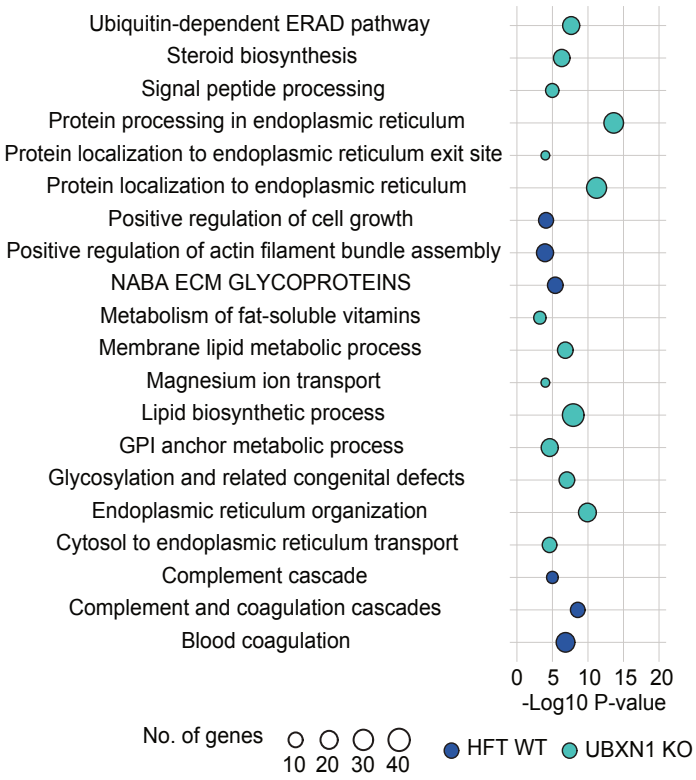

Supplementary Figure 4

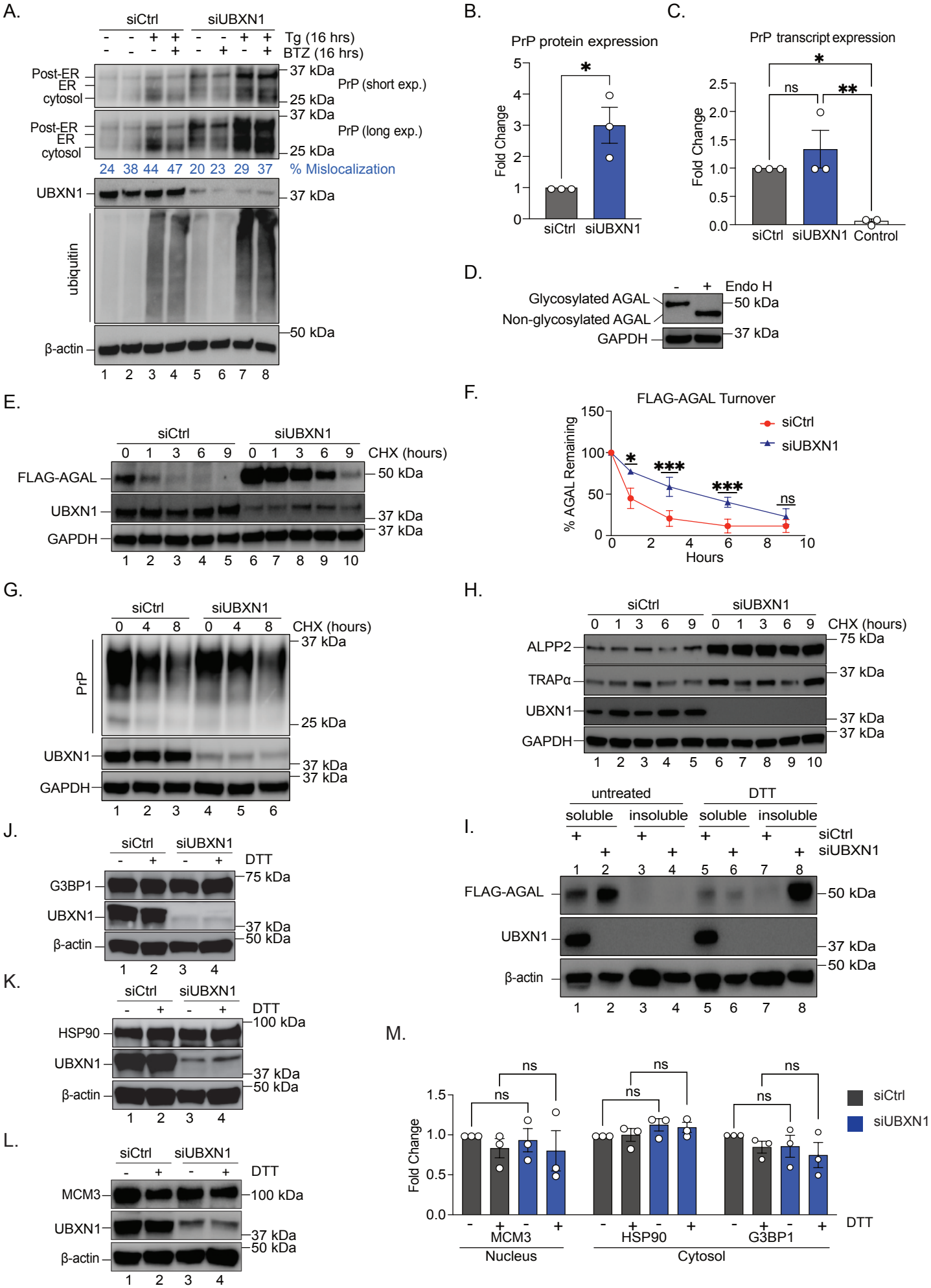

Supplementary Figure 5

A.

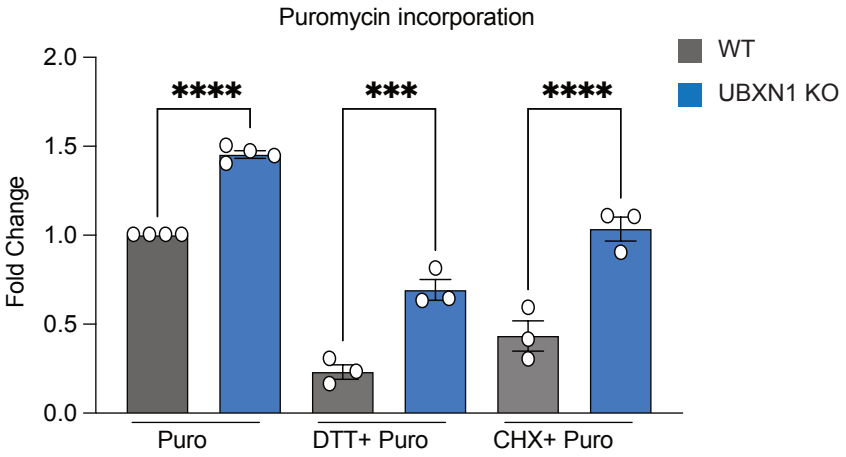

B.

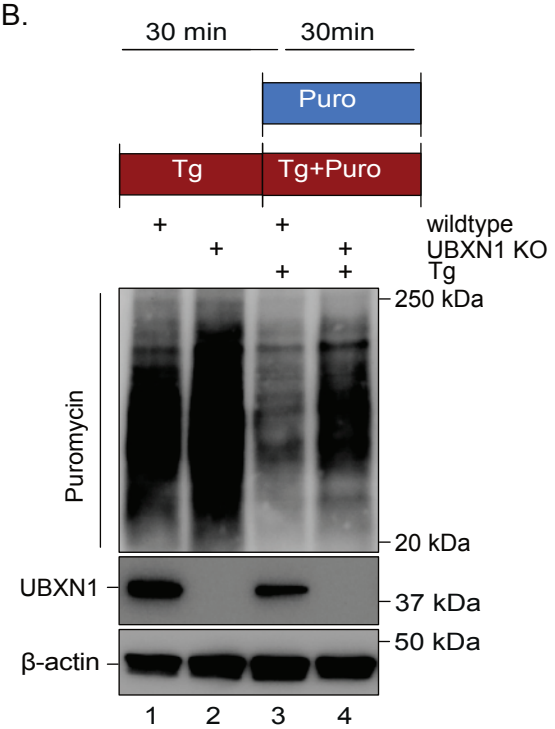

C.

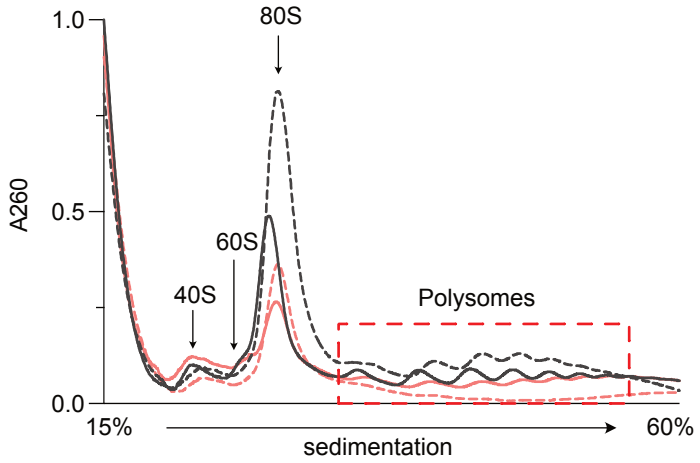

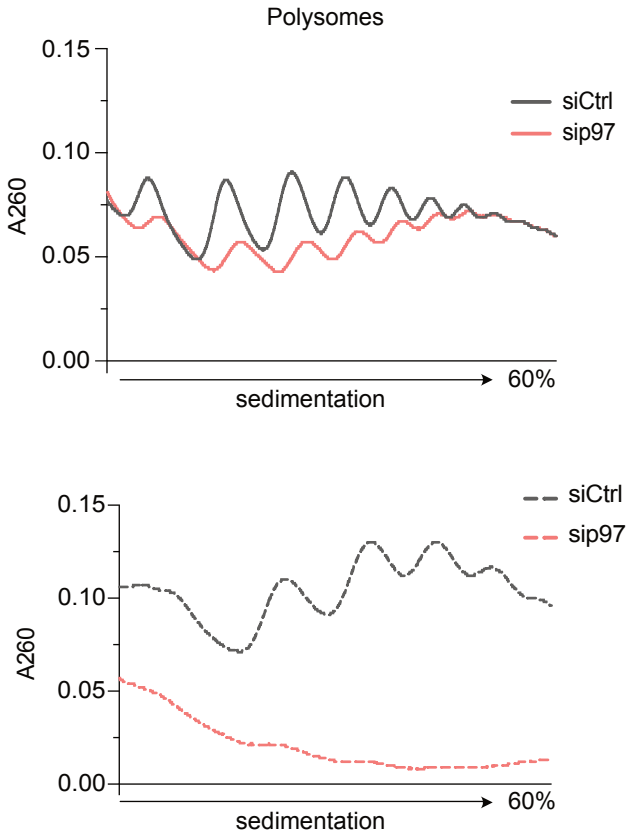
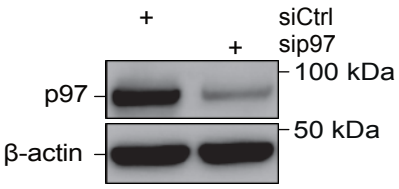
D.